Journal of Molecular Science

Journal of Molecular Science
Volume 35 Issue 4, Year of Publication 2025, Page 1678-1698
DoI-10.004687/1000-9035.2025.219

Journal of Molecular Science
www.jmolecularsci.com ISSN:1000-9035

A comprehensive Study on *Dalbergia Sissoo* bark for Pharmacognostic, Antimalarial evaluation, and Molecular Modelling

Dr. Pradip Ghogare[1], Sujata Lambe[2], Bhavana Tambe [3], Dr. Vijay Tambe[4], Nilesh narode[5], Vaishali Borade[3]

[1] Department of Pharmacognosy, SMBT College of Pharmacy, Dhamangaon, Tal-Igatpuri, Dist. Nashik-422403.
[2] Department of Pharmaceutical chemistry, SMBT College of Pharmacy, Dhamangaon, Tal-Igatpuri, Dist. Nashik-422403.
[3] Institute of diploma Pharmacy Dhamangaon, Tal-Igatpuri, Dist.Nashik-422403.
[4] College of Pharmacy (D. Pharm& B. Pharm) A/P-Chincholi-Mohu, Sinnar Dist., Nashik-422102
[5] Department of Pharmaceutics, Amrutvahini College of Pharmacy, Sangamner, Dist. Ahmednagar-422403.

Article Information
Received: 04-10-2025
Revised: 22-10-2025
Accepted: 17-11-2025
Published: 26-12-2025

Keywords
Dalbergia Sissoo extracts; Antimalarial activity of quercetin; Pharmacognostic screening; HPTLC standardization; Molecular docking and dynamic simulation; Network pharmacology

ABSTRACT

The bark of *Dalbergia Sissoo* is traditionally used for the treatment of many diseases such as malaria. Despite its traditional relevance, the pharmacognostic parameters and pharmacological properties remained unexplored. In this study, we aim to develop the missing pharmacognostic parameters with modern analytical techniques and carry out multi-step computational studies to study the antimalarial potential of *D. Sissoo*. The bark was 2–6 mm thick, composed of different colored layers, and was bitter-sweet in taste. Powdered microscopy revealed the presence of starch granules, calcium oxalate crystals, cork cells, trichomes, and fibers. Physicochemical properties such as ash values (total, acid-insoluble, and water-soluble), extractive values (petroleum ether, chloroform, ethyl acetate, methanol, aqueous, 80% MeOH), moisture content, swelling index, fluorescence, and pH of the bark were determined. FT-IR fingerprint profiling of petroleum ether, chloroform, ethyl acetate, methanol, aqueous, and 80% MeOH extracts revealed characteristic bands at different wavelengths that are indicative of the presence of certain functional groups. HPTLC fingerprint profiling with a mobile phase of hexane: ethyl acetate: formic acid (4.5:5.5:0.5 v/v) revealed 9 characteristic peaks. With a mobile phase of toluene: ethyl acetate: formic acid (5:4:0.2 v/v), the validated TLC densitometric studies revealed the presence of 2.07 mg of quercetin (*Rf* = 0.477 ± 0.005) in 100 mg of 80% MeOH bark extract of *D. Sissoo*. Jaz QSAR web tool predicts the IC_{50} of quercetin against *Plasmodium falciparum* as 3.88 ± 0.35 µM, which was not far from the practically observed value for quercetin. Multi-target molecular docking with a validated docking protocol revealed that quercetin could potentially interact with 20 proteins of *P. falciparum* that are highly expressed during the schizont and trophozoite stages. Network pharmacology studies revealed that quercetin could potentially alleviate malaria mainly by inhibiting pro- inflammatory response through the action of IL-4, IL-10, and IL-13 and by triggering the immune system. The pharmacognostic parameters of *D. Sissoo* bark may be used as quality control parameters to aid in identification and authentication and to prevent adulteration. The results obtained from the multi-target molecular docking and network pharmacology studies support the use of *D. Sissoo* as a traditional herbal remedy against malaria.

Journal of Molecular Science
Journal of Molecular Science
Volume 35 Issue 4, Year of Publication 2025, Page 1678-1698
DoI-10.004687/1000-9035.2025.219

INTRODUCTION:

Dalbergia Sissoo Roxb. is an evergreen tree that is distributed in Southeast Asian countries such as foothills of the Himalayas ranging from Afghanistan in the west to Bihar, India, in the east. It also occurs naturally in Iran. It is primarily found growing along river banks above 200 m (700 ft) elevation, but can range naturally up to 1,400 m (4,600 ft) [1]. *D. Sissoo* is traditionally used as a herbal rem- edy for the treatment of certain ailments. The stem bark of *D. Sissoo* was traditionally used by the Mizo tribe of India to treat inflammation of glands, pregnant women with inflammation, sickness, and mange [2]. Another study reported that the Mizo tribe of India used the decocted bark extract of *D. Sissoo* to treat dysentery and tonsillitis [3]. In Meghalaya, the bark is prepared with a decoction process, and the extract is used to treat indigestion [4]. In Thailand, the fruit of *D. Sissoo* was taken raw to treat stomach ache [5]. Despite the traditional relevance of *D. Sissoo* as a herbal medicine, the quality control param- eters of *D. Sissoo* are not available. Moreover, the phytochemical profile and pharmacological activity of the plant remained uninvestigated.

The traditional pharmacognostic parameters such as macroscopy (thickness, color, odor, taste, presence of foreign organic matter and fracture), microscopy (transverse section, characteristics of powdered drug such as color, odor, histochemical analysis, and fluo- rescence), and physicochemical parameters (total ash, extractive values, moisture content, swelling index, pH and fluorescence analysis of extracts) played an impor- tant role to control the quality of a crude drug [6]. In the absence of organoleptic features, pharmacognostic parameters such as microscopy and physicochemical properties can aid in the identification and authentica- tion of a crude drug [7]. Following the trend, modern analytical techniques are now used to develop differ- ent quality control parameters of a crude drug. The fin- gerprint profile of a herbal extract developed with the Fourier transform infrared (FT-IR) technique and can be used for the assessment of the purity of a herbal extract, detection of adulterants, identification of the potential functional groups of phytocompounds present in a herbal extract, detection of impurities, and act as a referential monograph to aid in quality control of a crude drug [8]. Similarly, the fingerprint profile of a herbal extract developed with the high-performance thin-layer chromatography (HPTLC) technique can be used for the assessment of the purity of a herbal extract, act as a referential monograph to aid in quality control of a crude drug, and development of a validated method for the quantification of phytomarkers for the standardization of a crude drug [9, 10].

A survey conducted with a traditional practitioner in Maharashtra by the first author revealed that the bark of *D. Sissoo* was traditionally used as a herbal remedy to treat malaria. Malaria is a para- sitic disease caused by *Plasmodium* parasites, namely *P. falciparum*, *P. vivax*, *P. malariae*, *P. knowlesi*, and *P. berghei* [11]. Among the parasites, the most severe form of malaria is caused by *Plasmodium falciparum* [11]. According to the World Malaria Report 2023, a total of 249 million cases of malaria were reported in the year 2022 [12]. Studies have reported the rise of drug-resist- ant *Plasmodium* strains against the first line of malarial treatment, namely artemisinin-based combination therapies [13]. The problem of drug resistance coupled with the toxicity and low bioavailability of the current antimalarial drugs has created a situation wherein the need to find newer alternatives with higher bioavailabil- ity, higher efficacy, and lower toxicity has gained trac- tion [13, 14]. Auspiciously, medicinal plants have been a reservoir of bioactive compounds with potent phar- macological activities since ancient times [15]. Interest- ingly, two of the most effective antimalarial compounds such as quinine and artemisinin were isolated from tra- ditional medicinal plants [16, 17]. Based on these, it is logical to study the antimalarial properties of *D. Sissoo* with *in silico* techniques such as molecular dock-ing and network pharmacology.

Molecular docking is a useful computational tech- nique that is used to study the molecular interactions between a compound and a protein. Molecular docking provides an idea of the binding affinity of a compound toward the active binding site of a protein. A good binding affinity, i.e., low binding energy, correlates to a favorable binding pose over other poses of the same compound. Through molecular docking studies, the type of protein–ligand interactions such as conventional hydrogen bonds and hydrophobic or electrostatic interactions are revealed [18]. In this study, molecular docking studies will reveal the potential targets of *D. Sissoo* against *P. falciparum*. Network pharmacology is used to identify the potential molecular mechanism of action by statistically correlating the possibility of interactions by a chemical against multiple genes in a disease pathway. The effect of a chemical or the potential gene targets in different metabolic pathways can be identified through network pharmacology studies. Network

Journal of Molecular Science
Volume 35 Issue 4, Year of Publication 2025, Page 1678-1698
DoI-10.004687/1000-9035.2025.219

pharmacology has been widely used in the field of drug repurposing for the identification of new targets in a different disease other than what it was originally studied for [19]. In this study, network pharmacology studies will reveal the potential molecular mechanism of action of *D. Sissoo* through the identification of potential gene targets in the human malaria pathway.

In this study, we will develop the pharmacognostic parameters of the bark of *D. Sissoo* through the utilization of classical pharmacognostical studies an modern analytical techniques. Since it was reported to the authors that the bark of *D. Sissoo* was traditionally used by the Mizo tribe to treat malaria, a study on the antimalarial potential of quercetin identified in the 80% MeOH bark extract of *D. Sissoo* will be carried out. *In silico* techniques such as molecular docking and network pharmacology studies will provide valuable insights into the antimalarial properties of *D. Sissoo*. Molecular docking studies will be used to identify the potential targets of quercetin against multiple proteins that are expressed during the trophozoite and schizont stages of *P. falciparum*. Network pharmacology will help us to bet- ter understand the traditional effectiveness of *D. Sissoo* against malaria at the molecular level.

METHODS:

A flowchart for the materials and method section was prepared, and it is provided in the supplementary file as Figure s1.

Collection and taxonomical identification:

The medicinal plant was collected with the help of a local guide. The World Health Organization (WHO) guidelines on good agricultural and collection practices (GGACP) were followed during the collection of the medicinal plant part. A herbarium with a standard sheet size of 11.5 inches × 16.5 inches was prepared for identifi- cation by a registered taxonomist.

Macroscopy and microscopy:

The thickness, surface characteristics, color, fracture, odor, and taste of the bark were documented according to existing protocols [20, 21]. The presence of foreign organic matter was determined according to the standard protocols given in the Indian Pharmacopoeia [22]. The crude drug was then ground into fine pow- der. The color and the odor of the powdered drug were documented. The transverse section (TS) of the bark was stained with iodine and sudan red, and it was observed under a light microscope under different ranges of magnifications. Histochemical analysis was carried out by staining the powdered bark with different reagents. The microscopical parameters were identified with a Projec- tion microscope (Systonics). For fluorescence analysis, common laboratory reagents were added to the powdered bark, and they were observed under daylight, at 254 nm, and 366 nm.

Physicochemical properties:

The total ash, acid-insoluble ash, and water-soluble ash were determined according to standard procedures described in different literature [23]. The extractive values of the bark of *D. Sissoo* were calculated according to the protocols described in the Indian Pharmacopoeia [22]. The moisture content and the swelling index of the bark of *D. Sissoo* were calculated according to the standard protocols [24]. The ultraviolet (UV) cabinet of Coslab was used to analyze the fluorescence of five extracts, namely petroleum ether, chloroform, ethyl acetate, methanol, aqueous, and 80% methanol that were prepared through the direct maceration technique. The pH of the bark was determined with a glass pH elec- trode (Equiptronics, Chandivali Mumbai) that can detect a pH range of −1.999 to 19.999.

Fourier transform infrared analysis of the organic bark extracts:

FT-IR spectroscopy is an analytical technique that is widely used for quality control in pharmaceutical indus- tries [25]. FT-IR analysis of six extracts, namely petro- leum ether, chloroform, ethyl acetate, methanol, aqueous, and 80% methanol extracts of *D. Sissoo,* was carried out with Bruker FT-IR Alpha-E Spectrometer. The spectra were measured with the OPUS Version 7.0 Build 7, 0, 129 (20,111,219) software. The resolution was set at 4 cm^{-1}, and the sample scan time and background scan time were both kept at 24 scans. The spectra were recorded within a range of 4000 cm^{-1} to 500 cm^{-1}. For the data blocks to be saved, we selected transmittance, single channel, and background.

High-performance thin-layer chromatography studies HPTLC is a simple and effective technique for the devel- opment of quality control parameters. In addition, it can be used to detect the presence of adulterants and to check the rate of degradation of a herbal extract. An HPTLC system of CAMAG equipped with a CAMAG TLC scanner, Vision CATS 3.2 SP 2 software, and LINO- MAT 5 applicator attached with a 100 µl syringe was used to study the 80% MeOH extract. The HPTLC studies were carried out at a 22°C with a relative humidity of 55%. The 80% MeOH extract was selected based on the results of trials and errors. During multiple trails, it was observed that the 80% MeOH had the highest number of peaks. In addition, method validation for the quanti- fication of quercetin was properly achieved with the 80% MeOH extract.

Development of HPTLC fingerprint profile of 80% MeOH:

A concentration of 30 mg/ml of 80% MeOH extract with methanol as the solvent was prepared with the

Journal of Molecular Science
Volume 35 Issue 4, Year of Publication 2025, Page 1678-1698
DoI-10.004687/1000-9035.2025.219

aid of a vortex machine. This was first followed by centrifugation for 5 min at 2000 revolutions per minute and then filtra- tion with a syringe filter (0.22 µm). A TLC silica gel 60 F_{254} plate (10 × 10 cm) was used as the stationary phase. Hexane: ethyl acetate: formic acid (4.5:5.5:0.5 v/v) was used as the mobile phase, and a twin-trough-chamber (10 × 10 cm) with a saturation time of 20 min was selected as the development chamber. The sample was applied to a total of 7 tracks (2.0 µL, 3.0 µL, 4.0 µL, 5.0 µL, 6.0 µL, 7.0 µL, and 8.0 µL). Detailed protocols including the scanner specifications are provided in the supplementary file.

Development and method validation for the quantification of quercetin in 80% MeOH extract of D. Sissoo

The reagents and solvents used in the present study were of analytical grade, and they were obtained from Merck (Mumbai, India). Quercetin was procured from Sigma-Aldrich (Mumbai, India). The stock solutions of the sample and the standard were freshly prepared daily throughout the study. The reagents and solvents were directly used without further purification or testing.

Sample and standard preparation With the aid of a vor- tex machine, 30 mg of 80% MeOH extract was dissolved in 1 ml of MeOH to obtain a concentration of 30 mg/ ml. Similarly, 1 mg of quercetin was dissolved in 1 ml of MeOH to obtain a concentration of 1 mg/ml. The sam- ple and the standard were dissolved in a microcentrifuge tube. Then, they were centrifuged for 5 min at 2000 revo- lutions per minute. After centrifugation, the supernatants were filtered with a syringe filter (0.22 µm).

Mobile phase and development chamber A solvent com- bination of toluene: ethyl acetate: formic acid (5:4:0.2 v/v) with a total volume of 10 ml was used to develop the TLC plate. CAMAG glass twin-trough-chamber (TTC) with a size of 10 × 10 cm was used as the development chamber. The mobile phase was equally distributed in equal volumes to the front trough (5 ml) and the rear trough (5 ml) of the TTC. A saturation pad (Whatman filter paper) was kept on the front trough to aid in chamber saturation. A total of 20 min was adopted as the saturation time.

Stationary phase A TLC silica gel 60 F254 was obtained from Merck. The size of the plate was adjusted to 10 × 10 cm. To remove dirt particles and fingerprints, the TLC plate was washed with a combination of methanol: chloroform (50:50 v/v).

Sample application With a 100-µL syringe (Hamil- ton), the samples were applied to the TLC plate with the CAMAG Linomat V semi-automatic Sample Spotter The dosage speed was 150 nL/s, and the pre-dosage volume was 0.20 µL. The sample and standard were applied at a height of 8 mm (Y-axis). The length of the band was 8 mm, while the width was 0. The first band was applied at 15 mm (X-axis) from the edge, and a distance of 10 mm was kept between each band. The bands were developed to a height of 70 mm.

After development, the TLC plate was dried with a hair dryer. Derivatization was not performed since the bands were visible under daylight and at 254 nm when observed under the UV Cabinet Chamber. Owing to this, it was possible to obtain the λ_{max} of the standard and the sample in their natural conditions.

With the CAMAG TLC scanner, quantitative analysis of the standard and the sample was performed by scan- ning the plates at 254 nm. The presence of quercetin in 80% MeOH was confirmed through the superimposition of the UV spectra of the standard and the sample within the same R_f 0.477 ± 0.005 window.

Calibration curve of quercetin Quercetin content in the sample was determined with a calibration curve that was established with the standard concentration ranging from 2000 to 10,000 ng/band. The calibration curve of querce- tin was fitted with the linear regression model wherein the linearity of the curve will be assessed with the correlation coefficient (r^2) [26]. The CAMAG Linomat V semiauto- matic Sample Spotter was used to apply the stock solution in increasing volumes 2 µL (2000 ng/band), 4 µL (4000 ng/band), 6 µL (6000 ng/band), 8 µL (8000 ng/band), and 10 µL (10,000 ng/band).

Validation of the HPTLC method According to the Inter- national Conference on Harmonization (ICH) guidelines, the developed HPTLC method was validated through dif- ferent tests such as linearity, robustness, reproducibility, precision (repeatability), limit of detection, limit of quan- tification, and accuracy (recovery). Detailed protocols are provided in the supplementary file.

***In vitro* antimalarial screening of quercetin**

Preparation of standard drug and quercetin

Quercetin was prepared in stock solutions of 1 mg/ml with incomplete RPMI-1650 media containing 0.5% DMSO as the solvent. Following the same protocol, a stock solution of 100 µg/ml was prepared for chloro- quine phosphate.

In vitro culture of malaria parasites:

Two strains of *P. falciparum*, namely 3D7 (chloroquine- sensitive) and RKL-9 (chloroquine-

resistant), obtained from the Parasite Bank of National Institute of Malaria Research (Indian Council of Medical Research), New Delhi, were maintained in fresh A + erythrocytes sus- pended in RPMI-1640 medium supplemented with 0.23% sodium bicarbonate, 1% D-glucose, 10% heat-inactivate.

AB +serum, 25 mM HEPES, amphotericin- B (0.25 mg/ ml), gentamycin (40 mg/ml) at 37 °C and 5% CO_2 environ- ment [27]. At 24-h intervals, fresh medium supplemented with 10% heat-inactivated AB +serum was used to replace the old medium while maintaining the parasitemia level below 2%.

Antimalarial activity screening:

Giemsa staining light microscopy method was used to screen quercetin against 3D7 and RKL-9 strains of *P. fal- ciparum*. Synchronization of the *P. falciparum* parasites to obtain the ring-staged parasitized cells was achieved with the treatment of 5% D-sorbitol. A complete medium and fresh A + erythrocytes were used to maintain the initial ring stage at a parasitemia of 0.5% in 4% hematocrit. In a 96-well plate, a twofold serial dilution method was followed to obtain nine different concentrations of quercetin and the standard drug. A concentration range of 50 to 0.19 µg/ ml and 5 to 0.019 µg/ml was obtained for quercetin and standard drug, respectively. The treatment was performed in triplicate. Following this, 20 µl of parasitized blood was added to wells containing 100 µl of quercetin and standard drug samples. A CO_2 incubator with a 5% CO_2 environ- ment was used to incubate the plates at 37 °C for 36–40 h. Glass slides were used to prepare blood smears from each well and methanol was used to fix the slides. Staining of the glass slides was achieved with 10% Giemsa stain prepared in 1% phosphate buffer solution. A light microscope (Leica DM1000) at 1000X (oil emersion) magnification was used to count the number of schizonts per 100 asexual parasites [28]. For each concentration, the following equation is used to calculate the percentage inhibition:

no.of schizontsin test quercetin identified in *D. Sissoo* against *P. falcipa- rum* and malaria.

Half-maximal inhibitory concentration (IC_{50}) prediction of quercetin against Plasmodium falciparum

Although the IC_{50} of quercetin against *P. falciparum* has

already been reported, we decided to put our previously developed QSAR models to the test. Initially, the 2D molecular descriptors of quercetin were calculated with the PaDEL descriptor software. The IC_{50} (Mean ± SD) of quercetin against *P. falciparum* was predicted with the JazQSAR web tool (https://etflin.com/software/JazQS AR). JazQSAR web tool uses three 2D-QSAR models that rely on a combination of different molecular descrip- tors to predict the *in vitro* antiplasmodial activity against *P. falciparum* [29]. The result of the JazQSAR web tool prediction is equivalent to the results obtained from the *in vitro* [^{3}H]-hypoxanthine incorporation assay, and the results were expressed as mean ± SD.

Multi-target molecular docking studies of quercetin against P. falciparum

Retrieval of druggable antiplasmodial targets The tropi-

cal disease research (TDR) database, which can be used as a tool to prioritize druggable targets from whole genomes, was used to identify the druggable targets of *P. falciparum*. Different filters were applied in the TDR database to filter out druggable targets from the whole genome of *P. falci- parum*. The targets were filtered based on the availability of the crystal structures in the Protein Data Bank (PDB) database. Under validation data, we select the 'any phar- macological validation' popping out from the pharmaco- logical validation option. The network drugability score

$$\%inhibition = 1 - \frac{}{no.of\ schizontsin\ negativecontrol\ X\ 100}$$

was set to a value of ≥ 3. The drugability score ranges from 1 to 5 , and a target with a higher drugability score is con- GraphPad Prism (GraphPad Prism v.8 Diego, Califor- nia, USA) was used to plot a nonlinear regression curve between the dose vs % inhibition, and finally, the IC_{50} val- ues were calculated and expressed as mean ± SD.

***In silico* studies:**

After quercetin was confirmed to be present in the 80% MeOH bark extract of *D. Sissoo*, we observed that quercetin was reported to inhibit the chloroquine- sen- sitive and chloroquine-resistant strains of *Plasmodium falciparum* with an IC_{50} value of 4.11 ± 2.05 µM and 2.94 ± 2.41 µM, respectively. The presence of quercetin partly explained the use of *D. Sissoo* as a traditional herbal remedy for the treatment of malaria. In the fol- lowing *in silico* studies, we will apply various techniques to increase our knowledge of themolecular effects of considered to be more druggable. Two datasets available in the TDR database, namely "New insights into the blood- stage transcriptome of *P. falciparum* using RNA-Seq" and "Data on upregulation of *P. falciparum* genes in different life cycle stages, combined from several microarray exper- iments available in PlasmoDB" were used to exhaustively screen the targets. In the first dataset, the intra-erythro- cytic stage at 24 h, 32 h, 40 h, and 48 h with all ranges of gene expression was considered. In the second data- set, the early and late trophozoite (~ 22.5 to ~ 32.5 h) and schizont stages (~ 32.5 to ~ 42.5 h) with all ranges of gene expression were considered [30, 31]. The common genes

from the two datasets were identified. Following this, the PDB ID of the proteins expressed by the genes was identi- fied from the PDB database. The PDB ID of proteins was considered only if they have a native ligand bound at the active site of the protein *Protein and ligand preparation* The 'Edit binding site' feature of the BIOVIA Discovery Studio Visualizer (DSV) software v.20.10.19295 was used to identify the binding site coordinates of the native ligands that were bound to the active binding site of the proteins [32]. In the absence of a native ligand, COACH-D can be used to identify the most suitable binding site of a protein [33]. The DSV software was used to remove the water molecules, heter- oatoms, and co-factors from the protein. Following this, hydrogen atoms were added to the protein with the DSV software. UCSF Chimera and Open Babel module of PyRx 0.8 are commonly used to optimize a ligand [34, 35]. The energy of quercetin and the positive controls were opti- mized with the Open Babel module of PyRx 0.8 by keep- ing the parameters default, namely, Force field = Universal Force Field; Optimization algorithm = Conjugate; Total number of steps = 200; Number of steps for update = 1; Stop if energy difference is less than = 0.1 [36]. The Open Babel version 3.1.1 software was used to protonate querce- tin and the co-crystal inhibitors (CCIs) at a pH of 7.4 to mimic the binding conditions of the human blood.

Molecular docking, docking validation, and analysis of results Finally, molecular docking simulation studies were carried out with the AutoDock Vina embedded in the PyRx 0.8 tool [37, 38]. Visualization and analysis of the 2D molecular interactions were carried out with the Lig- Plot + v.2.2.9 software [39,40]. The DockRMSD web tool (https://zhanggroup.org/DockRMSD/) was used to vali- date the docking protocol through the re-docking, super- imposition, and root-mean- square deviation (RMSD) calculation technique [41].

Prediction of potential gene targets for quercetin in malaria pathway through network pharmacology:
Since the presence of quercetin is confirmed in the 80% MeOH bark extract of *D. Sissoo*, we used the net- work pharmacology technique for two purposes: firstly to justify the use of *D. Sissoo* as a traditional herbal remedy for the treatment of malaria and secondly to understand the molecular mechanism of quercetin against malaria.

Identification of genes targeted by quercetin The target genes of quercetin were identified from various genomic databases such as HERB (http://herb.ac.cn/), Pharm- Mapper (https://www.lilab-ecust.cn/pharmmapper/) (zscore ≥ 1), SEA Search Server (https://sea.bkslab.org/) (zscore ≥ 0.1), STITCH (http://stitch.embl.de/), Super- PRED (https://prediction.charite.de/), and SwissTar- getPrediction (http://www.swisstargetprediction.ch/). 'Quercetin' was used as the search query in the databases. Deduplication was done to remove redundant genes, and the entire dataset was processed and standardized with the UniProt ID database (https://www.uniprot.org/).

Identification of genes associated with malaria The tar- get genes associated with malaria were retrieved from various online genomic databases such as the Compara- tive Toxicogenomics Database (https://ctdbase.org/), Dis- GeNET (https://www.disgenet.org/) (score ≥ 0.1), Gene cards (https://www.genecards.org/) (score ≥ 10), and OMIM (https://www.omim.org/). 'Malaria' was used as the search query in the databases. The malaria-associated genes identified from all the databases were combined, and deduplication was done to remove redundant genes. Then, all the genes were verified and standardized with the UniProt ID database (https://www.uniprot.org/).

Identification of common genes The gene targets that are common between quercetin targets and malaria-associ- ated genes were identified with the Venn Diagram Tool (https://bioinfogp.cnb.csic.es/tools/venny/).

Generation of protein–protein network and identifica- tion of hub genes The protein–protein interactions were generated with the STRING database (https://string-db. org/). The interactions between quercetin target genes and malaria-associated genes were visualized and ana- lyzed with the Cytoscape software (version 3.10.1) [42,43]. From the common genes, the cytohubba plugin of the Cytoscape software was used to rank the hub genes (top 10 genes) based on degree.

Gene ontology (GO) enrichment analysis The enrich- ment analyses were conducted with the GO and malarial molecular pathway enrichment analysis. The hub genes were used as the list of genes for GO enrichment analy- sis. DAVID database was used to process the hub genes to study the related biological processes (BP), molecular functions (MF), cellular compartments (CC), and KEGG analysis (https://david.ncifcrf.gov/). In addition, the KEGG mapper was used to visualize, identify, and color-code the most influenced genes in the malaria molecular pathway (https://www.kegg.jp/pathway/hsa05144). The results of the enrichment analyses were further visualized with the SRPlot tool (https://www.bioinformatics.com. cn/en).

RESULTS:

Collection and identification

With the help of a local guide the bark of *D. Sissoo*

Journal of Molecular Science
Volume 35 Issue 4, Year of Publication 2025, Page 1678-1698
DoI-10.004687/1000-9035.2025.219

was collected from the riverside of bhagur dist. Nashik Maharashtra India. The herbarium containing different plant parts of *D. Sissoo* was taxonomically identified and authenticated by Prof. S. S. Medakkar Head department of Botany Arts, science and commerce college Rahuri Dist. Ahmednagar M.S. (Letter No. 25/2009-10/201 dated 15/07/2009).

Macroscopy:
The bark of *D. Sissoo* consisted of different colored layers. The external part of the bark was greenish gray (ash-gray) in color, and the entire bark was consistently covered with tiny burls (small whitish bumps) that were either round or oval. The bark can be considered to be composed of four different layers based on differences in colors. The first layer of the bark was observed to have a dark green color, and it lies immediately beneath the external surface of the bark. The second layer of the bark was observed to have a fresh green color. The third layer of the bark was observed to have a light reddish-brown color. The fourth layer of the bark was observed to have a dark reddish-brown color. A range of 2–6 mm was ultimately established as the thickness of the bark after it was measured on different bark pieces. The fresh bark was flexible but the dried bark was brittle and splintery. The fresh bark was odorless but the dried bark had a char- acteristic smell. The fresh bark was bitter-sweet in taste. Upon chewing the fresh bark, the bitter-sweet taste per- sisted in the mouth for at least 15 min. There was no for- eign organic material present in the collected barks of *D. Sissoo*.

Microscopy:
The color of the powdered bark was greenish brown. However, reddish brown color was the most dominant color. Close inspection revealed that the powdered bark was a mixture of gray, green, brown, and brick-red colors. The powdered bark had a characteristic smell.

The TS of the bark is given in Fig. 2. The TS of the bark was stained with iodine and Sudan red. Iodine-stained TS of the bark was discarded from the study as it produced excessive bubbles, and capturing a good-quality image was not possible. The TS of the bark was analyzed at 4x, 10x, and 40 × magnification , respectively. Through this study, we observed the presence of cork cells (phellem) in the bark of *D. Sissoo*. The reddish and pinkish color indicates the presence of suberin in the cork cells. The results of the histochemical analysis of the powdered bark are given in Fig. 3. The presence of starch granules (Fig. 3(A)), calcium oxalate crystals (Fig. 3(A)), cork cells (Fig. 3(B)), trichome (Fig. 3(C)), and fibers (Fig. 3(D)) were identified with the help of a Projection microscope (Zeiss).

Staining of starch granules with iodine results in a blue to black-colored complex (Fig. 3(A)). The calcium oxalate crystals present in the bark of *D. Sissoo* have unique shapes. Some crystals are shaped like prisms (elongated rectangles, often hexagonal and varies in size), while others fall within the category of crystal sands (small crystals that do not have a defined shape) (Fig. 3(A)). Sudan red and phloroglucinol-HCl staining revealed the presence of cork cells in powdered microscopy (Fig. 2 (B, C) and Fig. 3(B)). After careful examination, the characteristic of the trichome detected in *D. Sissoo* was identified to be unicel- lular (filiform) (Fig. 3(C)). Based on the shape, it falls under the category of non-glandular trichomes with a sub-category of simple trichomes. The fiber detected in *D. Sissoo* appears to be liber (phloem) fibers as it is a slender, elongated, thickened wall with a tapered end (Fig. 3(D)).

The results of the fluorescence analysis of the powdered bark of *D. Sissoo* alone and after reac- tion with common laboratory agents are provided in the supplementary file Table s1. Initially, the fluorescence of the powdered drug was observed alone in the absence of chemical reagents. The powdered drug alone was greenish brown under daylight, gray under 254 nm (ultraviolet), and greenish gray (fluorescence) under 366 nm. After this, the powdered drug was made

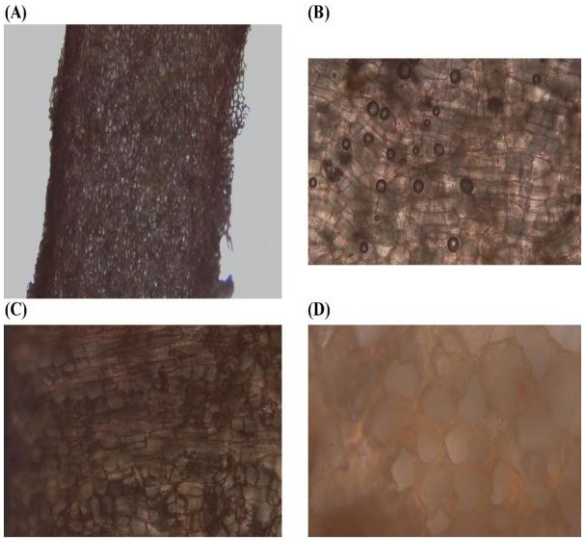

Fig. 2 (A) 4 × magnification of the TS of the bark, (B) 10 × magnification, (C) 40 × magnification, and (D) 40 × magnification of the very edge of the bark

Journal of Molecular Science
Journal of Molecular Science
Volume 35 Issue 4, Year of Publication 2025, Page 1678-1698
DoI-10.004687/1000-9035.2025.219

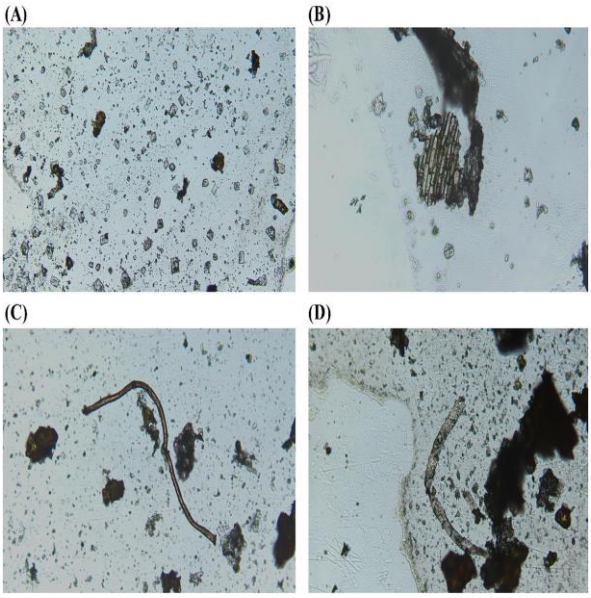

Fig. 3 (A) Calcium oxalate crystal, (B) cork cells, (C) trichome, and (D) fiber of *D. Sissoo* visualized under 10 × magnification

to react with a total of 20 chemical reagents. Different colors observed under daylight were greenish brown, blackish brown, brick red, greenish yellow, yellowish green, reddish brown, green, and yellowish brown. Dif- ferent colors observed under 254 nm were gray, black, dark purple, dark red, grayish black, brownish black, blackish gray, and dark brown. Fluorescence observed under 366 nm was greenish gray, black, dark red, gray- ish green, blackish gray, grayish black, and dark brown.

Physicochemical properties:

The physicochemical properties of medicinal plants are an important indication of their quality as external environmental factors can easily influence the physico- chemical properties of a medicinal plant [44].

Total ash calculations:

A total ash of 8.213% was present in 2 g of the pow- dered bark. Acid-insoluble ash constitutes 1.088% of the total ash, while water-soluble ash constitutes 4.716% of the total ash. The ash determination experi- ment was carried out only once.

Extractive values:

The extractive values were measured in triplicate. The extractive values of petroleum ether, chloroform, and ethyl acetate extracts were found to be 2 ± 0.5%. The extractive values of methanol, aqueous, and 80% MeOH extracts were found to be 6 ± 0.5%.

Moisture content:

A total of 0.1 g (6.6%) of moisture was reported to be present in 1.5 g of the powdered bark.

Swelling index:

The initial height of 1 g of coarsely grounded bark before the addition of water was 0.85 cm. The initial volume occupied by the dried bark was calculated with the formula: Volume = $\pi r^2 h$. The radius of the stop- pered cylinder was 0.95 cm. After calculation ($3.14 \times (0.95)^2 \times 0.85$), the initial volume occupied by the dried bark was found to be 2.40 cc. The final height of 1 g of the bark in a 25-ml stoppered cylinder after the addition of water was 1.5 cm. The final volume occu- pied by the dried bark was calculated to be 4.25 cc. The initial volume was subtracted from the final volume. Finally, the swelling index of the bark of *D. Sissoo* was found to be 1.85 cc.

Fluorescence of extracts:

The results of the fluorescence analysis of the extracts are provided in the supplementary file Table s2. The char- acteristic of each extract concerning its adhesiveness/ viscosity is also highlighted in the supplementary file Table s2. Under daylight, the petroleum ether, chloro- form, ethyl acetate, methanol, aqueous, and 80% MeOH extract were found to be yellowish brown, dark green, light green, greenish brown, reddish brown, and reddish brown, respectively. Under 254 nm, the petroleum ether, chloroform, ethyl acetate, methanol, aqueous, and 80% MeOH extract were found to be yellowish brown (dark), brownish purple, wine red (dark), grayish green, blackish purple, and greenish purple, respectively. Under 366 nm, the petroleum ether, chloroform, ethyl acetate, metha- nol, aqueous, and 80% MeOH extract were found to be yellowish brown (light), pinkish purple, wine red (light), grayish green, greenish purple, and greenish purple, respectively. The petroleum ether was found to be slightly sticky, while the chloroform, ethyl acetate, and aqueous extract were found to be sticky semi-solid. Upon drying, the methanol and 80% MeOH extract were found to hard and non-sticky. However, penetrating the hard extract revealed that the inner part of the methanol and 80% MeOH extract were slightly sticky.

pH of the bark:

The pH of the tap water and distilled water ranged from 6.5 to 7. After the powdered bark of *D. Sissoo* was added, the pH of the tap water and distilled water was found to be 5.5. The change in the pH of the tap water and distilled water could be due to the presence of cer- tain phytochemicals.

FT-IR analysis:

The functional groups of the phytochemicals present in the herbal extracts (petroleum ether, chloroform, ethyl acetate, methanol, and 80% MeOH) were analyzed based on the band values identified in the FT-IR spectrum. In the FT-IR spectra, the wave number (cm^{-1}) is given on the x-axis and the transmittance (%) is given on the y-axis. The FR-IR spectra of all the bark extracts of Dalbergia Sissoo are given in Fig. 4.

Journal of Molecular Science
Volume 35 Issue 4, Year of Publication 2025, Page 1678-1698
DoI-10.004687/1000-9035.2025.219

FT-IR spectra of petroleum ether extract:

The FT-IR spectrum of the petroleum ether extract of *D. Sissoo* labeled with their corresponding band numbers is given in Fig. 4 (A). A detailed analysis of the bands, functional groups, and possible compounds iden- tified in the petroleum ether extract of *D. Sissoo* is given in the supplementary file Table s3.

A total of 10 bands were identified between 1500–500 cm^{-1}. The first band observed at 538.25 cm^{-1} indicates C–Cl stretching of alkyl halides. The second band observed at 722.81 cm^{-1} indicates CH_2 bending of alkane. The third band observed at 818.48 cm^{-1} indicates the N–H bending of amine. The fourth band observed at 977.75 cm^{-1} indicates the C–H bending of methyl. The fifth band observed at 1019.37 cm^{-1} indicates C–O–C stretching of the ketone. The sixth band and seventh band observed at 1103.82 cm^{-1} and 1167.34 cm^{-1}, respec- tively, indicate C–C stretching of ketone. The eighth band observed at 1247.87 cm^{-1} indicates C–O stretch- ing of alcohol. The ninth and tenth bands observed at 1374.49 cm^{-1} and 1457.29 cm^{-1}, respectively, indicate C–H bending of methyl.

A total of 2 bands were observed between 2000– 1500 cm^{-1}. The first band observed at 1513.36 cm^{-1} indicates N–H stretching of amine. The second band observed at 1727.90 cm^{-1} indicates C = O stretching of aldehyde. There were no bands observed between 2500–2000 cm^{-1}.

A total of 3 bands were observed between 3500– 2500 cm^{-1}. The first band observed at 2855.68 cm^{-1} indicates C–H stretching of methyl. The second band observed at 2923.15 cm^{-1} indicates N–H stretching of amine salt. The third band observed at 3398.56 cm^{-1} indicates N–H stretching of primary amine.

FT-IR spectra of chloroform extract:

The FT-IR spectrum of the chloroform extract of *D. Sissoo* labeled with their corresponding band numbers is given in Fig. 4(B). A detailed analysis of the bands, functional groups, and possible compounds identified in the chloroform extract of *D. Sissoo* is given in the supplementary file Table s4.

A total of 12 bands were observed between 1500– 500 cm^{-1}. The first band observed at 566.09 indicates the C–Cl stretching of alkyl halide. The second band and third band observed at 722.27 cm^{-1} and 753.09 cm^{-1}, respectively, indicate C–H bending of the aromatic ring. The fourth, fifth, and sixth bands observed at 819.55, 882.11, and 980.42 cm^{-1}, respectively, indicate C–H bending of alkene. The seventh band observed at 1029.48 cm^{-1} indicates C–O–C stretching of dialkyl. The eighth band observed at 1121.81 cm^{-1} indicates the

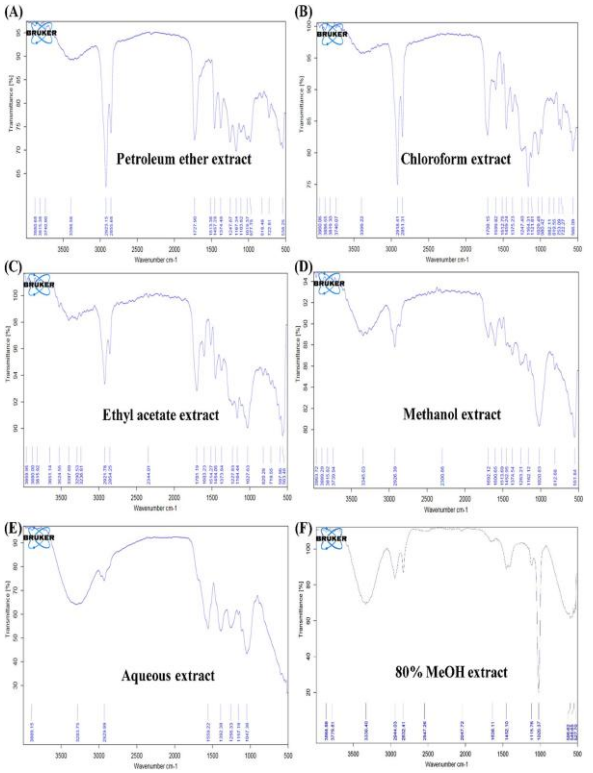

Fig. 4 FT-IR spectra of (A) petroleum ether extract; (B) chloroform extract; (C) ethyl acetate extract; (D) methanol extract; (E) aqueous extract; and (F) 80% MeOH extract C–C stretching of the ketone. The ninth band observed at 1164.31 cm^{-1} indicates C–O stretching of ester. The tenth band observed at 1247.40 cm^{-1} indicates C–O–C stretching of ester. The eleventh band observed at 1375.23 cm^{-1} indicates CH_3 bending of alkene. The twelfth band observed at 1459.24 cm^{-1} indicates CH_2 bending of alkene.

A total of 3 bands were observed between 2000– 1500 cm^{-1}. The first and second bands observed at 1512.75 and 1599.82 cm^{-1}, respectively, indicate N–H bending of amine. The third band observed at 1708.15 cm^{-1} indicates C = O stretching of the ketone. There were no bands that were detected between 2500–2000 cm^{-1}.

A total of 3 bands were observed between 3500– 2500 cm^{-1}. The first and second bands observed at 2851.31 and 2918.41 cm^{-1}, respectively, indicate C–H stretching of alkene. The third band observed at 3399.22 cm^{-1} indicates O–H stretching of alcohol.

FT-IR spectra of ethyl acetate extract:

The FT-IR spectrum of the ethyl acetate extract of *D. Sissoo* labeled with their corresponding band numbers is given in Fig. 4(C). A detailed analysis of the bands, functional groups, and possible compounds identified in the ethyl acetate extract of *D. Sissoo* is given in the supplementary file Table s5.

A total of 9 bands were observed between 1500– 500 cm^{-1}. The first band observed at 563.46 cm^{-1} indicates C–Cl stretching of alkyl halide. The second band.

Journal of Molecular Science
Journal of Molecular Science
Volume 35 Issue 4, Year of Publication 2025, Page 1678-1698
DoI-10.004687/1000-9035.2025.219

FT-IR spectra of methanol extract:

The FT-IR spectrum of the methanol extract of *D. Sissoo* labeled with their corresponding band numbers is given in Fig. 4(D). A detailed analysis of the bands, func- tional groups, and possible compounds identified in the methanol extract of *D. Sissoo* is given in the supple- mentary file Table s6.

A total of 7 bands were observed between 1500– 500 cm^{-1}. The first band observed at 551.84 cm^{-1} indicates C–Cl stretching of alkyl halide. The second band observed at 812.68 cm^{-1} indicates the C–H bend- ing of the aromatic ring. The third band observed at 1020.83 cm^{-1} indicates C–F stretching of alkyl halide. The fourth band observed at 1162.12 cm^{-1} indicates C–C

(O) –C stretching of ester. The fifth band observed at 1263.21 cm^{-1} indicates C–N stretching of amine (aryl).

The sixth band observed at 1374.54 cm^{-1} indicates

observed at 597.96 cm^{-1} indicates the C–Cl stretching of acid chloride. The third and fourth bands observed stretching of the aromatic ring. The fifth band observed−1could be interpreted as a functional group.

A total of 3 bands were observed between 2000–

at 1027.63 cm indicates C–O stretching of ester.

1500 cm^{-1}. The first band observed at 1513.69 cm^{-1} indi-

The sixth and seventh bands observed at 1164.44 and 1227.83 cm^{-1}, respectively, indicate C–C (O) –C stretch- ing of ester. The eighth band observed at 1373.84 cm^{-1} indicates the CH_3 bending of alkane. The ninth band observed at 1454.05 cm^{-1} indicates CH_2 bending of alkane.

A total of 3 bands were observed between 2000– 1500 cm^{-1}. The first band observed at 1514.27 cm^{-1} indicates N–H bending of amide. The second band observed at 1603.23 cm^{-1} indicates C–C stretching of the aromatic ring. The third band observed at 1701.19 cm^{-1} indicates C = O stretching of carboxylic acid. Between 2500– 2000 cm^{-1}, a single band at 2344.01 cm^{-1} was observed. However, this specific wave number did not fall within any particular range that could be interpreted as a func- tional group.

A total of 7 bands were observed between 3650– 2500 cm^{-1}. The first band observed at 2854.25 cm^{-1} indicates C–H stretching of aldehyde. The second band observed at 2921.78 cm^{-1} indicates C–H stretching of alkene. The third and fourth bands observed at 3236.81 and 3290.53 cm^{-1}, respectively, indicate N–H stretching of amide. The fifth band observed at 3397.69 cm^{-1} indi- cates O–H stretching of alcohol. The sixth band observed at 3524.55 cm^{-1} indicates N–H stretching of amide. The seventh band observed at 3651.14 (equivalent to 3650) cm^{-1} indicates the O–H stretching of alcohol.

cates N–H bending of amide. The second band observed at 1600.65 cm^{-1} indicates C = C stretching of the aro- matic ring. The third band observed at 1692.12 cm^{-1} indicates R_2C = N–R stretching of amide. Between 2500– 2000 cm^{-1}, a single band was observed at 2300.86 cm^{-1}. However, this particular wave number did not fall within any particular range that could be interpreted as a func- tional group.

A total of 2 bands were observed between 3500– 2500 cm^{-1}. The first band observed at 2926.39 cm^{-1} indicates C–H stretching of alkane. The second band observed at 3345.03 cm^{-1} could potentially indicate either the O–H stretching of carboxylic acid or the N–H stretching of amide.

FT-IR spectra of aqueous extract

The FT-IR spectrum of the aqueous extract of *D. Sissoo* labeled with their corresponding band numbers is given in Fig. 4(E). A detailed analysis of the bands, func- tional groups, and possible compounds identified in the aqueous extract of *D. Sissoo* is given in the supple- mentary file Table s7.

A total of 4 bands were observed between 1500– 500 cm^{-1}. The first band observed at 1047.36 cm^{-1} indicates S = O stretching of sulfoxide. The second band observed at 1157.19 cm^{-1} indicates S = O stretching of sulfone. The third band observed at 1256.33 cm^{-1} indicates C–C(O) –C stretching of ester. The fourth band observed at 1392.38 cm^{-1} indicates the C–H bending of alkenes. A single band of 1559.22 cm^{-1} was observed between 2000–1500 cm^{-1}

indicating an N–H bending of amide. There was no band observed between 2500–2000 cm^{-1}.

A total of 2 bands were observed between 3500– 2500 cm^{-1}. The first band observed at 2929.99 cm^{-1} indicates the C–H stretching of alkanes. The second band observed at 3283.75 cm^{-1} indicates O–H stretching of carboxylic acid.

FT-IR spectra of 80% MeOH extract

The FT-IR spectrum of the 80% MeOH extract of *D. Sissoo* labeled with their corresponding band numbers is given in Fig. 4(F). A detailed analysis of the bands, functional groups, and possible compounds identified in the 80% MeOH extract of *D. Sissoo* is given in the supplementary file Table s8.

A total of 6 bands were observed between 1500–

500 cm^{-1}. The first band observed at 527.70 cm^{-1} indicates the C–Br stretching of alkyl halide. The second band observed at 546.65 cm^{-1} indicates the C–Cl stretching of alkyl halide. The third band observed at

596.62 cm^{-1} indicates the C–H bending of alkyne. The fourth band observed at 1020.37 cm^{-1} indicates C–N stretching of alkyl amine. The fifth band observed at

Journal of Molecular Science
Volume 35 Issue 4, Year of Publication 2025, Page 1678-1698
DoI-10.004687/1000-9035.2025.219

1115.76 cm^{-1} could potentially indicate either C–N stretching of amine or C–O stretching of anhydride or C–C stretching of ketone. The sixth band observed at 1452.10 cm^{-1} indicates CH_2 bending of alkane. Between 2000–1500 cm^{-1}, a single band was observed at 1638.11 cm^{-1}, which indicates C = C stretching of alkene. The band of 2047.72 cm^{-1} observed between 2500–2000 cm^{-1} did not fall within any particular range that could be interpreted as a functional group.

A total of 4 bands was observed between 3500– 2500 cm^{-1}. The first band observed at 2547.26 cm^{-1} indicates O–H stretching of carboxylic acid. The second band observed at 2832.41 cm^{-1} indicates the C–H stretching of alkane. The third band observed at 2944.03 cm^{-1} indicates C–H stretching of alkane. The fourth band observed at 3330.40 cm^{-1} could potentially indicate either the O–H stretching of carboxylic acid or the N–H stretching of amide.

HPTLC fingerprint profile of 80% MeOH bark extract of *D. Sissoo*

The fingerprint profile of the 80% MeOH extract of *D.Sissoo* developed with hexane: ethyl acetate: formic acid (4.5:5.5:0.5 v/v) as the mobile phase is given in Fig. 5. The TLC plates visualized under 366 nm are given in Fig. 5(A). In Fig. 5(A), we can observe the presence of several phytochemicals as evidenced by the separation of the 80% MeOH extract into multiple bands. A total of 8 tracks with increasing volumes were applied across the

TLC plate and it can be seen that 2 µL was not sufficient to yield distinctively visible bands after development with the mobile phase. However, 8 µL yielded bands that were distinctively visible under 366 nm after plate devel- opment. In Fig. 5(B), the evaluated 2D-chromatogram (8 µL) of the 80% MeOH extract is provided. A total of 9 peaks were detected by the VisionCATS 3.2 SP 2 soft- ware. The retention factor (Rf) of each peak was given on the X-axis, while the concentration of each peak was given on the Y-axis.

The Rf and the area covered by each peak are given in the supplementary file Table s9. The area of the peak correlates to the concentration of the phytochemical present in the extract, i.e., the larger the area, the higher the concentration, and vice versa. Peak 8 has the high- est area % of 20.62 with a Rf of 0.905 followed by peak 4 (area % = 17.98%, Rf = 0.506), peak 6 (area % = 16.60%,

Rf = 0.685), peak 7 (area % = 16.36%, Rf = 0.840), peak

5 (area % = 10.58%, Rf = 0.552), peak 1 (area % = 8.60%,

Rf = 0.021), peak 9 (area % = 6.69%, Rf = 0.985), peak 2 (area % = 1.88%, Rf = 0.068), and peak 3 (area % = 0.69%, Rf = 0.148).

Method development and validation for quantification of quercetin in 80% MeOH bark extract of *D. Sissoo*

After the TLC plate was developed to a height of 70 mm, the R_f values of the resolved bands were observed. The photograph of the TLC plate consisting of the bands of quercetin and 80% MeOH extract of the bark of *D. Sissoo* under daylight and UV at 254 nm is given in Fig. 6. The 3D densitometric chromatogram of querce- tin and 80% MeOH extract of *D. Sissoo* at 254 nm are also given in Fig. 6. The R_f of quercetin was found to be 0.477 ± 0.005. The R_f value of quercetin matched with the R_f value of the 80% MeOH bark extract of *D. Sissoo*, which was found to be in the window of 0.477. The spectra of quercetin and 80% MeOH extract of the bark of *D. Sissoo* measured within the range of 190 nm to 450 nm matched upon superimposition, and this confirms the presence of quercetin in the test sample (Fig. 6). The calibration curve of quercetin is given in Fig. 6. The calibration function obtained was $y = 2.319 \times 10^{-8}x + 1.945 \times 10^{-2}$. The regression data denote a satisfactory linear relationship for the concentration ranging from 2000–10000 ng/band. The coefficient of variation was 4.22%, and the correlation coefficient was 0.994843. The high correlation coefficient value indicates the lin- earity of the calibration curve and the adherence of the HPTLC system to Beer's law [45].

The method validation parameters for the quantification of quercetin in 80% MeOH extract of *D. Sissoo* by TLC Densitometric method are given in Table 1, and the recovery studies are given in the supplementary

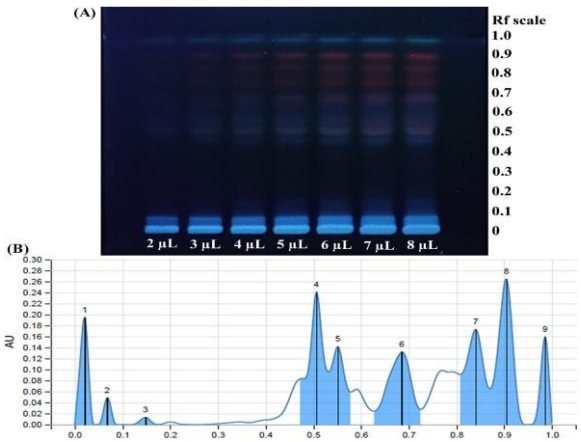

Fig. 5 (**A**) Visualization of TLC plate with separated bands under 366 nm; (**B**) evaluated 2D-chromatogram (8 µL) of the 80% MeOH extract. The retention factor of each peak is given on the X-axis, while the concentration of each peak is given on the Y-axis

file Table s10. The intraday (CV = 4.22%) and interday (CV = 4.57%) results suggested that the HPTLC method was precise and reproducible. The LOD and LOQ values of quercetin were found to be 2.090 and 4.440 µg/band, respectively. The accuracy

Journal of Molecular Science
Volume 35 Issue 4, Year of Publication 2025, Page 1678-1698
DoI-10.004687/1000-9035.2025.219

of the HPTLC method was suggested by the average percentage recovery of querce- tin (92.13% ± 1.40), which lies within the acceptable lim- its. The low %CV value ascertained the reproducibility and robustness of the HPTLC method and suggested that quercetin was stable during the analytical study. Based on the TLC densitometric method, a total of 2.07 mg of quercetin was found to be present in 100 mg of 80% MeOH bark extract of *D. Sissoo*.

Fig. 6 Visualization of TLC plate under (**A**) daylight and (**B**) UV wherein 1, 2, 3, 4, 5, 6, 7, and 8 represents Track 1 with an applied volume of 2 µL (2000 ng/band) followed by Track 2 = 4 µL (4000 ng/band); Track 3 = 6 µL (6000 ng/band); Track 4 = 8 µL (8000 ng/band); Track 5 = 10 µL (10,000 ng/ band); Track 6 = 4 µL; Track 7 = 6 µL; and Track 8 = 8 µL. Tracks 1 to 5 represent quercetin and tracks 6 to 8 represent 80% MeOH bark extract of *D. Sissoo*. (**C**) 3D densitometric chromatogram of quercetin and 80% MeOH bark extract of *D. Sissoo* at 254 nm with an *Rf* window of 0.477.
(**D**) Superimposition of absorption spectra of quercetin and 80% MeOH bark extract of *D. Sissoo*. (**E**) Calibration curve of quercetin

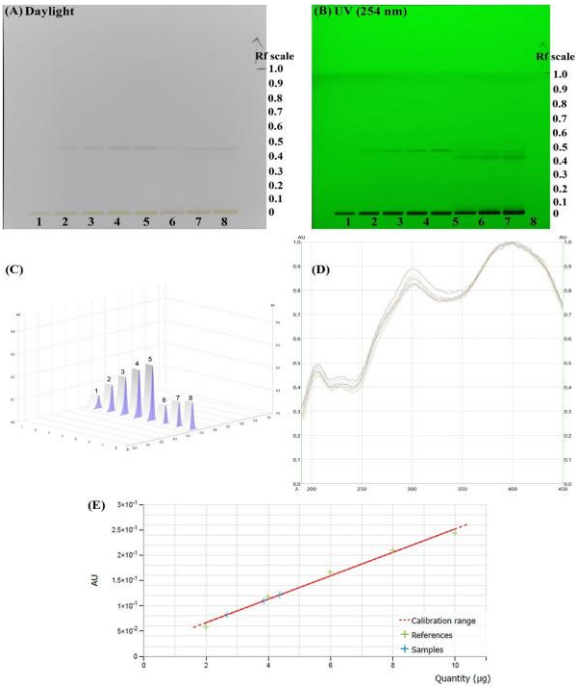

Fig. 6 (See legend on previous page.)

Table 1 Method validation parameters for the quantification of quercetin in 80% MeOH extract of *D. Sissoo* by TLC densitometric method

Parameters	Observed data	Acceptance criteria
Linearity	2000 ng to 10,000 ng/band	Linear, accurate, and precise
Correlation coefficient	0.99483	0.9–1.1
Linear regression equation	y = 2.319 × 10–8 x + 1.945 × 10–2	
Coefficient of variation	4.22%	Herbal extracts = < 5%
LOD	2.090 µg/band	
LOQ	4.440 µg/band	
Percentage recovery (Accuracy)	92.13% ± 1.40	Within 90–110%
Reproducibility	3.94%	Herbal extracts = < 5%
Robustness	3.74%	Herbal extracts = < 5%
Intraday (Precision) (n = 3)	4.22%	Herbal extracts = < 5%
Interday (Precision) (n = 3)	4.57%	Herbal extracts = < 5%

2D-molecular descriptors of quercetin used for the IC_{50} prediction are provided in the supplementary file.

Multi-target molecular docking studies of quercetin against P. falciparum targets

In the next step, we aim to identify the potential molecu- lar targets of quercetin in *P. falciparum*. This study will enhance our understanding of the antiplasmodial activity of quercetin.

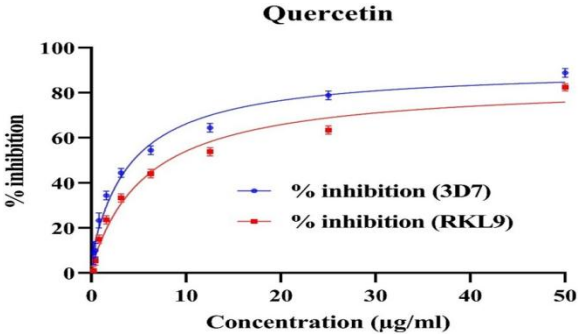

Fig. 7 Percentage inhibition of quercetin at 50 µg/ml, 25 µg/ml, 12.5 µg/ml, 6.25 µg/ml, 3.12 µg/ml, 1.56 µg/ml, 0.78 µg/ml, 0.39 µg/ ml, and 0.19 µg/ml

***In vitro* antimalarial screening of quercetin against *P. falciparum*:**

The dose vs % inhibition of quercetin against *P. falcipa- rum* is given in Fig. 7. The IC_{50} of quercetin against 3D7 and RKL-9 strain of *P. falciparum* was calculated to be 4.45 ± 1.40 µg/ml and 5.94 ± 0.91 µg/ml, respectively.

IC_{50} prediction of quercetin against *P. falciparum*:

After the presence of quercetin was confirmed to be pre- sent in the bark of *D. Sissoo* through the HPTLC technique, we used an in-house developed web tool to predict the biological activity of quercetin against *P. falciparum*. The JazQSAR web tool predicted the IC_{50} of quercetin as 3.88 ± 0.35 µM against *P. falciparum*. This partly explains the use of the bark of *D. Sissoo* as a traditional herbal remedy against malaria. The

Retrieval of druggable P. falciparum targets

From the 'New insights into the blood-stage transcrip- tome of *P. falciparum* using RNA-Seq' dataset, a total of 38 genes with an expression percentile of 0–100 was identified to be expressed at 24, 32, 40, and 48 h.

Journal of Molecular Science
Volume 35 Issue 4, Year of Publication 2025, Page 1678-1698
DoI-10.004687/1000-9035.2025.219

From the 'Data on upregulation of *P. falciparum* genes in dif- ferent life cycle stages, combined from several microar- ray experiments available in PlasmoDB' dataset, a total of 65 genes with an expression percentile of 0–100 was identified to be expressed during the early and late schiz- ont and trophozoite stages. Then, 38 common genes were identified from the two datasets. Finally, based on the availability of a CCI which will serve as a positive control and which will also be used for docking protocol valida- tion, a total of 24 genes that express druggable *P. falcipa- rum* proteins were selected for the multi-target molecular docking studies. Details of the selected gene ID, PDB ID, and protein name are provided in the supplementary file.

Molecular docking:

The CCIs are used as a positive control, and their bind- ing affinity was used as a benchmark to assess the per- formance of quercetin. The binding affinity of quercetin and the CCIs against their respective protein is provided in Table 2. Out of a total of 24 targets, quercetin was able

Table 2 Binding affinity of quercetin and the CCIs of each protein

PDB ID	Quercetin (-kcal/mol)	CCIs (-kcal/mol)
1CET	−7.2	−5.7
1Q1G	−9.5	−7.7
1Q4J	−8.2	−4.6
1RL4	−7.5	−4.9
1UH5	−9.0	−7.3
1V0O	−9.5	−10.8
1VYQ	−6.6	−4.2
1LS5	−8.0	−7.5
2B4R	−7.9	−3.3
4Z22	−8.5	−6.7
2HTE	−8.3	−6.2
2PMN	−8.5	−7.2
2QAF	−7.7	−7.3
3BPF	−8.0	−5.4
3EBH	−8.5	−8.1
3I65	−9.8	−11.1
3KR4	−7.9	−7.5
3OZG	−10.9	−8.8
3QGT	−8.8	−4.6
3QS1	−7.2	−9.3
3WQR	−8.3	−6.5
5JWC	−6.5	−4.5
6M2L	−8.8	−5.8
7DIJ	−6.9	−6.9

to outperform the CCIs of 20 proteins in terms of hav- ing a better binding affinity at the active site of the pro- tein. Among the 20 proteins, quercetin showed the best binding affinity with 3OZG (−10.9 kcal/mol), followed by 1Q1G (−9.5 kcal/mol), 1UH5 (−9.0 kcal/mol), 3QGT (−8.8 kcal/mol), 6M2L (−8.8 kcal/mol), 4Z22 (−8.5 kcal/ mol), 2PMN (−8.5 kcal/mol), 3EBH (−8.5 kcal/mol), 2HTE (−8.3 kcal/mol), 3WQR (−8.3 kcal/mol), 1Q4J (−8.2 kcal/mol), 1LS5 (−8.0 kcal/mol), 3BPF (−8.0 kcal/ mol), 2B4R (−7.9 kcal/mol), 3KR4 (−7.9 kcal/mol), 2QAF (−7.7 kcal/mol), 1RL4 (−7.5 kcal/mol), 1CET (−7.2 kcal/ mol), 1VYQ (−6.6 kcal/mol), and 5JWC (−6.5 kcal/mol). However, quercetin was unable to outperform the CCIs of 1V0O, 3I65, 3QS1, and 7DIJ in terms of having a better binding affinity.

Based on the binding affinity, the 2D molecular interac- tions of quercetin with the 20 proteins were analyzed and the results are provided in Fig. 8. A systematic analysis of the molecular interactions is provided in the supplemen- tary file Table s11. Quercetin was able to form conven- tional hydrogen bonds with the majority of the studied proteins. The highest number of conventional hydrogen bond was formed with a total of 9 active site residues of 2QAF followed by 1UH5 (n = 8), 3OZG (n = 8), 3BPF (n = 6), 3I65 (n = 5), 3WQR (n = 6), 1CET (n = 5), 1Q1G (n = 5), 1VYQ (n = 5), 2HTE (n = 5), 6M2L (n = 5), 1LS5 (n = 4), 1Q4J (n = 4), 2BR4 (n = 4), 2PMN (n = 4), 5JWC (n = 4), 1V0O (n = 3), 3EBH (n = 3), 3KR4 (n = 3), 3QS1 (n = 3), 1RL4 (n = 2), 3QGT (n = 2), 7DIJ (n = 2), and 4Z22
(n = 0). In addition to conventional hydrogen bonds, quercetin also interacted with the active site residues of the protein through hydrophobic interactions.

The docking protocols for the 24 proteins were vali- dated with the re-docking, superimposition, and RMSD calculation techniques. The superimposed CCIs are graphically represented in supplementary file Figure s2. The RMSD between the binding pose of the CCIs gen- erated after molecular docking and the original bind- ing pose of the CCIs that are present at the active binding pocket of the proteins was calculated. The RMSD between the original CCI and the re-docked CCI for all the proteins was below 2.0 Å. The lowest and highest RMSD values were shown by the CCIs of 3WQR (RMSD = 0.302 Å) and 1LS5 (RMSD = 1.977 Å), respectively.

Prediction of potential gene targets for quercetin in malaria pathway through network pharmacology:

From a total of 6 databases, the total number of genes targeted by quercetin was found to be 349 genes. A total of 179 genes were found to be associated with malaria after screening 4 genomic databases. The total number of intersecting genes from these two groups was found to be 27, accounting for 5.5% of the total genes (Fig. 9).

A protein–protein interaction network was constructed with the 27 intersecting genes in the STRING data- base, which was sent for visualization in the Cytoscape software. A network of 27 nodes with 216 edges was observed as a result of close interactions between the genes (Fig. 10(A)). With 'degree' used as the ranking algo- rithm, a total of 10 genes were identified as the hub genes (Fig. 10(B)). The highest- ranked hub gene was IFNG fol- lowed by IL1B, TNF,

Journal of Molecular Science
Volume 35 Issue 4, Year of Publication 2025, Page 1678-1698
DoI-10.004687/1000-9035.2025.219

IL6, IL10, ICAM1, CXCL8, IL2, VCAM1, and CCL2.

The results of the GO enrichment analysis can be visualized in supplementary file Figure s3 wherein the top 10 most significant BP, CC, and MF are given. From Figure s3(A), we found that the most significant (p-value < 0.05) BP was inflammatory response followed by positive regulation of IL-6 production, cellu- lar response to lipopolysaccharide, leukocyte cell–cell adhesion, regulation of insulin secretion, positive regu- lation of IL-8 production, positive regulation of tran- scription from RNA polymerase II promoter, immune response, positive regulation of gene expression and neutrophil chemotaxis.

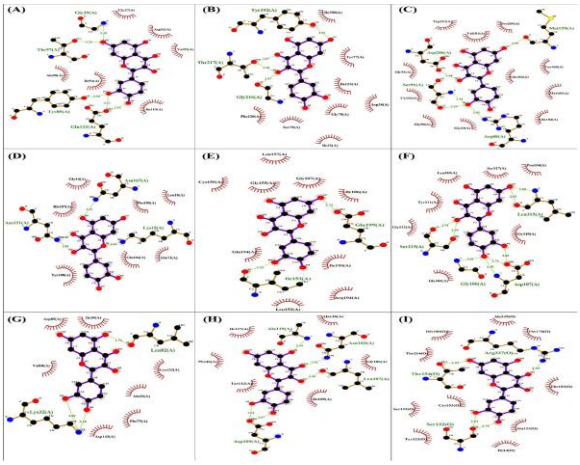

Fig. 8 Graphical representation of the 2D molecular interactions between quercetin and the active site residues of *P. falciparum* proteins namely (A) 1CET, (B) 1LS5, (C) 1Q1G, (D) 1Q4J, (E) 1RL4, (F) 1UH5, (G) 1V0O, (H) 1VYQ, (I) 2B4R, (J) 2HTE, (K) 2PMN, (L) 2QAF, (M) 3BPF, (N) 3EBH, (O) 3I65, (P) 3KR4, (Q) 3OZG, (R) 3QGT, (S) 3QS1, (T) 3WQR, (U) 4Z22, (V) 5JWC, (W) 6M2L, and (X) 7DIJ

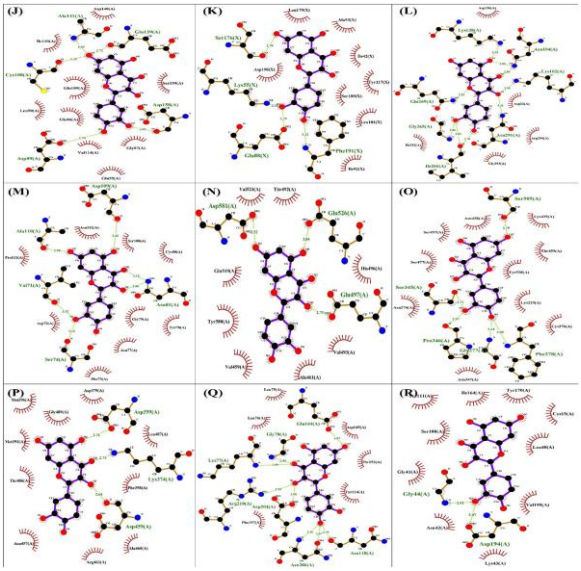

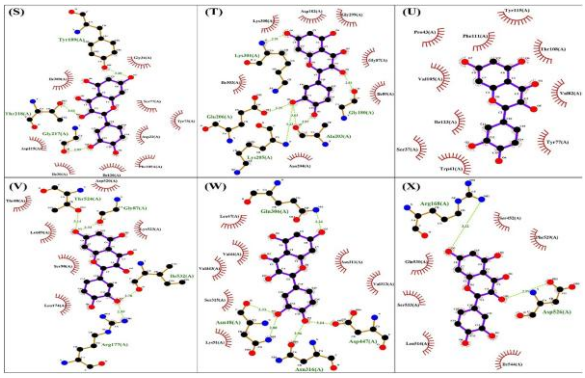

Fig. 8 continued

From Figure s3(B), we found that the most significant (p-value < 0.05) CC was extracellular space followed by the external side of the plasma membrane, extracellu- lar region, cell surface, cortical cytoskeleton, and mem- brane raft.

From Figure s3(C), the most significant (p-value < 0.05) MF was found to be cytokine activity followed by inte- grin binding, growth factor activity, chemokine activity, protein binding, CXCR chemokine receptor binding, identical protein binding, transmembrane signaling receptor activity, phospholipase binding, and TNF recep- tor binding.

KEGG and Reactome were used for pathway enrichment analysis, and the results are graphically presented in supplementary file Figure s4. The pathway enrichment analysis with KEGG revealed that malaria ranked 1st among the top 10 most significant pathways (Figure s4(A)). In addition, malaria has the highest fold enrich- ment and gene count (n = 13). This suggests the poten- tially significant role of quercetin identified in the bark of 80% MeOH bark extract of *D. Sissoo* in the molecular pathway of malaria. From Figure s4(B), the Reactome analysis for quercetin targets revealed that the most sig- nificant pathway was IL-4 and IL-13 signaling followed by IL-10 signaling, signaling by interleukins, cytokine signaling in immune system, immune system, interferon gamma signaling, CD163 mediating an anti-inflamma- tory response, parasitic infection pathways, Leishmania infection, and RUNX1 and FOXP3 control the develop- ment of regulatory T lymphocytes (Tregs).

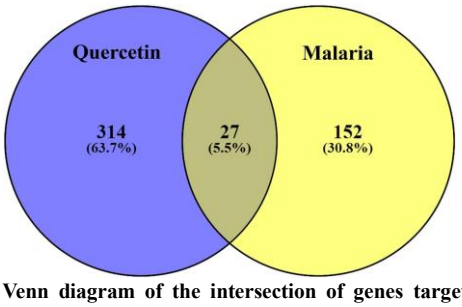

Fig. 9 Venn diagram of the intersection of genes targeted by quercetin and genes associated with malaria

Journal of Molecular Science
Journal of Molecular Science
Volume 35 Issue 4, Year of Publication 2025, Page 1678-1698
DoI-10.004687/1000-9035.2025.219

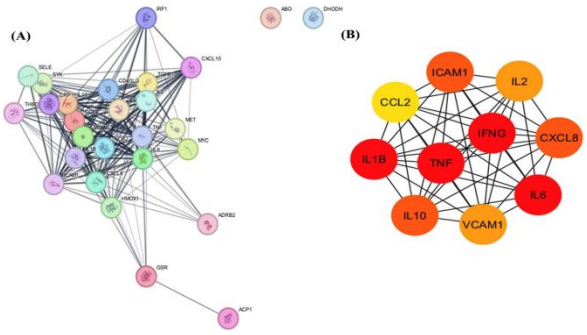

Fig. 10 (A) Protein–protein interactions among the common genes and (B) the network of the 10 hub genes

The KEGG pathway enrichment analysis revealed a total of 13 malaria-associated genes, namely IL10, TGFB1, VCAM1, CXCL8, SELE, TNF, ICAM1, IL6, CD40LG, IFNG, IL1B, CCL2, and MET (Figure s4(A)). A total of 10 hub genes, which are the common targets for quercetin and malaria-associated genes, are already given in Fig. 10B). The intersection of the two groups of genes (13 KEGG genes and 10 hub genes) revealed 9 intersect- ing genes accounting for 64.3% of the total, and along with this, the potential targets of quercetin in the malaria pathway are illustrated in supplementary file Figure s5. The study revealed that CXCL8, TNF, CCL2, ICAM1, IL6, IL1B, IFNG, VCAM1, and IL10 could potentially play a key role in alleviating malaria through the action of quercetin.

DISCUSSION:

Studies of all types related to medicinal plants always start with collection. In this study, the WHO-GGACP for medicinal plants was strictly followed during the collec- tion of the medicinal plant part to prevent exploitation and sustain the local ecosystem. The collection of the medicinal plant part was carried out with the assistance of a local guide. The next challenge after collection was taxonomical identification as it is an integral part of the quality control for a medicinal plant [20]. A herbarium consisting of the leaves and branches including the origi- nal images of the tree was sent for taxonomical identifi- cation. The tree from which the medicinal plant part was collected was taxonomically identified and authenticated as *D. Sissoo*.

Consumption of a misidentified plant with poisonous metabolites can have serious or sometimes, fatal conse- quences [46]. Therefore, the next challenge in our study was to develop quality control parameters that could potentially be used as a referential herbal monograph for the bark of *D. Sissoo*. A good herbal monograph should contain information that can be used to ade- quately define the physical features of a crude drug. The availability of a herbal monograph with adequate quality control parameters can be used to prevent misidentifica- tion [47]. In this study, we developed several quality con- trol parameters that could be used as a referential herbal monograph for the bark of *D. Sissoo*. We docu- mented several macroscopic parameters (organoleptic properties), microscopic parameters, and physicochemi- cal parameters.

The macroscopic features and microscopic features of the bark of medicinal plants will vary mainly based on their species, geographical location, chemical com- position, environmental stress, and ecological interac- tions [48]. The appearance, color, surface characteristics, texture, thickness, odor, and taste of the bark of *D. Sissoo* were documented. These macroscopic features are unique to the bark of *D. Sissoo* and can be used to differentiate it from other medicinal plants. In the absence of crude drugs without identifiable organoleptic properties, microscopical features can aid in powdered drug identification and detection of adulterants. In Fig. 2, the reddish and pinkish color of the cork cells (bark) indi- cates the presence of suberin which is a complex long- chain fatty acid that contributes to the waterproofing properties of a bark [49].

Some phytochemicals show fluorescence in the visible range of daylight. In addition, many phytocompounds can exhibit fluorescence during and after exposure to ultraviolet light and sometimes, the application of differ- ent reagents can convert phytocompounds to fluorescent derivatives. The qualitative evaluation of crude drugs has been carried out through this method and is considered to be an important part of pharmacognostical characteri- zation [50]. The fluorescence of the powdered drug and the extracts of *D. Sissoo* under daylight, 254 nm, and 366 nm could be mainly attributed to the reaction between the phytocompounds of the bark and the rea- gents. In addition, it could also be due to the formation of a fluorescent complex. Other factors such as changes in pH, polarity, and stabilization of the excited state can also impact the fluorescence.

Ash values such as total ash value, acid-insoluble ash value, and water-soluble ash value are considered impor- tant parameters to assess the purity, quality, mineral con- tent, and potential adulteration of plant-based medicinal drugs [51]. The total ash value represents the total quan- tity of inorganic residues of the bark. The acid-insolu- ble ash value constitutes a portion of the total ash that is insoluble in dilute hydrochloric acid such as siliceous or earthy matter [52]. The water-soluble ash value indi- cates the presence of water-soluble salts as it represents a portion of the total ash that is soluble in water [53]. The extractive values quantify the amount of phytoconstitu- ents extracted from a crude drug with a specific solvent, providing a measure of the quality, purity, and

potency of the medicinal drug derived from the plant [54]. The mois- ture content of bark indicates the amount of water and volatile matter present in the plant material [55]. Deter- mination of the moisture content is important as exces- sive moisture can lead to microbial growth, degradation, and reduced shelf life which can affect the quality and efficacy of medicinal preparations. The swelling index is a reflection of the mucilage content of a bark [54]. The decrease in the pH of tap water from 6.5 to 5.5 after the addition of the powdered crude drug could be due to the extraction of phytochemicals into the tap water.

FT-IR spectroscopy is used to identify functional groups of chemicals, and the non-destructive approach has made it an ideal technique for quality control pur- poses in food, beverage, and pharmaceutical industries [56]. The application of FT-IR spread rapidly due to its high speed, high repeatability, easy operation, low noise, and low expense. FT-IR also proved to be invaluable for the evaluation of herbal products [56]. The FT-IR finger- print profile of herbal extracts obtained from medicinal plants has been generated for its application as a quality control parameter. A study also concluded that herbal drugs can be identified based on the characteristic peaks of their FT-IR spectra. In this study, we have developed FT-IR fingerprints for petroleum ether, chloroform, ethyl acetate, methanol, and 80% MeOH bark extract of *Dalbergia Sissoo*. We can use these fingerprints as a reference to aid in identification, check for potential adulteration, and detect the presence of impurities. Moreover, based on Fig. 4, we can interpret the FT-IR spectra and use the functional groups to predict the phytocompounds that could potentially be present in the extracts.

The HPTLC fingerprint analysis plays an important role in the quality control of herbal medicines [57, 58]. When we carry out chromatographic and spectral analy- sis of the HPTLC fingerprint profile with a definite set of parameters, we can observe that a specified mobile phase has generated characteristic peaks that are unique to the 80% MeOH bark extract of *D. Sissoo*. The detec- tion of multiple peaks with different R_f indicates that the phytoconstituents of the extract separated based on the polarity of the mobile phase and stationary phase. Thus, the HPTLC fingerprint analysis revealed the presence of several phytoconstituents in the 80% MeOH bark extract as evidenced by the 9 peaks (Fig. 5). Similar to FT-IR fin- gerprinting, the developed HPTLC fingerprint profile can serve as a referential standard to check the purity of the extract, aid in identification, and check for potential adulteration.

After HPTLC fingerprinting, we developed and vali- dated an HPTLC densitometric method for the quanti- fication of quercetin in the 80% MeOH bark extract of *D. Sissoo*. The developed HPTLC method was found to be accurate, precise, robust, and reproducible for the determination of quercetin. This study has reported the presence of quercetin in 80% MeOH bark extract of *D. Sissoo* for the first time which makes our findings relevant. The developed HPTLC densitometric analysis can be used as a marker for quality control and for the standardization of the crude drug viz-a-viz quercetin. As shown in Fig. 6(E), the high value of the correlation coef- ficient (r^2 = 0.994843) indicates good linearity and peak homogeneity. The developed method was observed to have a low noise level as evidenced by the LOD and LOQ
values (Table 1). We have established a validated method for the quantification of quercetin and validation studies showed that the developed method was precise under the given set of experimental conditions.

Prediction of the biological activity of compounds with 2D-QSAR modeling saves time and money and provides accurate results rapidly. In the context of malaria, *in vitro* antimalarial screening requires an expensive laboratory setup and the time to complete the entire screening pro- cess can take up to 3 weeks. Previously, we developed three 2D-QSAR models and integrated them into a sim- ple web tool for the prediction of the IC_{50} of flavonoids against *P. falciparum* [29]. Using the three QSAR models, the JazQSAR web tool calculates the IC_{50} of flavonoids based on the specified 2D molecular descriptors, and the results are expressed as Mean ± SD. The result of the prediction is equivalent to the results obtained with the in vitro [^{3}H]-hypoxanthine incorporation assay. A study that uses a different technique of antiplasmodial screen- ing had previously reported quercetin to inhibit the chloroquine-sensitive and chloroquine-resistant strains of *P. falciparum* with an IC_{50} value of 4.11 ± 2.05 µM and 2.94 ± 2.41 µM, respectively. Our JazQSAR web tool pre-dicted the IC_{50} of quercetin to be 3.88 ± 0.35 µM against *P. falciparum*. Interestingly, the Giemsa light staining microscopy technique of *in vitro* antimalarial screen- ing revealed the IC_{50} of quercetin against 3D7 and RKL-9 strain of *P. falciparum* as 4.45 ± 1.40 µg/ml and 5.94 ± 0.91 µg/ml, respectively. The findings published by other researchers, the predicted IC_{50} with the JazQSAR web tool and the IC_{50} determined through the *in vitro* antimalarial screening showed great similarity. Since we had already confirmed the presence of quercetin in the 80% MeOH bark extract of *D. Sissoo* with the HPTLC technique, the results of the JazQSAR predic- tion and in vitro antimalarial screening supported the use of *D. Sissoo* as a traditional herbal remedy against malaria.

The authors of this study are aware that molecular docking studies of quercetin with *P. falciparum*

Journal of Molecular Science
Volume 35 Issue 4, Year of Publication 2025, Page 1678-1698
DoI-10.004687/1000-9035.2025.219

proteins have been carried out several times by other researchers [59–61]. Due to this, we used a different approach for our work. Molecular docking is used to study the molecular interactions between a compound and a protein [62]. In this study, we used the TDR web tool to retrieve 24 drug- gable proteins mainly based on the *P. falciparum* genes that are highly expressed during various stages. Before docking with quercetin, we validated the molecular dock- ing protocol for 24 proteins with the re-docking, super- imposition, and RMSD calculation technique (Fig. 9). Then, we found that quercetin could potentially interact with 20 proteins based on a higher binding affinity when compared with the positive controls (Table 2). Quercetin was able to form conventional hydrogen bonds, hydro- phobic interactions, electrostatic interactions, carbon- hydrogen bonds, and van der Waals forces with the active site residues of the studied proteins (Fig. 8). Although other types of interactions play a crucial role, conven- tional hydrogen bonds are one of the most important interactions as they are directly associated with the molecular recognition and catalytic activity of a protein [63].

The proteins whose positive control was outperformed by quercetin played an important role in the normal metabolic process of *P. falciparum*. Lactate dehydroge- nase (PDB ID: 1CET) catalyzes the interconversion of pyruvate and lactate with associated interconversion of NADH and NAD^+. Uridine phosphorylase (PDB ID: 1Q1G) catalyzes the phosphorolysis of uridine to ura- cil and ribose-1-phosphate. Glutathione s-transferase (PDB ID: 1Q4J) detoxifies endogenous and xenobiotic compounds by conjugation with glutathione. Formylme- thionine deformylase (PDB ID: 1RL4) removes the for- myl group from formylmethionine at the N-terminus of newly synthesized proteins. Enoyl-ACP reductase (PDB ID: 1UH5) plays a crucial role in fatty acid biosynthesis by catalyzing the reduction of enoyl-ACP to acyl-ACP. Deoxyuridine 5'-triphosphate nucleotide hydrolase (PDB ID: 1VYQ) hydrolyzes dUTP to dUMP and pyrophos- phate, preventing the incorporation of uracil into DNA. Plasmepsin IV (PDB ID: 1LS5) functions as an aspartic protease involved in hemoglobin degradation within the parasite's digestive vacuole. Glyceraldehyde-3-phosphate dehydrogenase (PDB ID: 2B4R) catalyzes the sixth step of glycolysis, converting glyceraldehyde 3-phosphate to 1,3-bisphosphoglycerate. Plasmepsin II (PDB ID: 4Z22) is an aspartic protease involved in the degrada- tion of the host hemoglobin [64]. Spermidine synthase (PDB ID: 2HTE) catalyzes the transfer of a propyl amine group from decarboxylated S-adenosylmethionine to putrescine, forming spermidine. Protein kinase 7 (PDB ID: 2PMN) is involved in various signaling pathways through phosphorylation of target proteins. Orotidine 5' monophosphate decarboxylase (PDB ID: 2QAF) cata- lyzes the decarboxylation of orotidine 5'-monophosphate to uridine monophosphate. Falcipain 2 (PDB ID: 3BPF) functions as a cysteine protease involved in hemoglobin degradation. M1 family aminopeptidase (PDB ID: 3EBH) plays a role in the final stages of hemoglobin degrada- tion by removing amino acids from peptide fragments. M17 leucyl aminopeptidase (PDB ID: 3KR4) functions in protein turnover by removing leucine residues from the N-terminus of peptides. Hypoxanthine–guanine-xanthine phosphoribosyl transferase (PDB ID: 3OZG) is involved in purine salvage by catalyzing the conversion of hypoxanthine, guanine, and xanthine to their respective ribonucleotides. Bifunctional dihydrofolate reductase- thymidylate synthase (PDB ID: 3QGT) catalyzes the reduction of dihydrofolate to tetrahydrofolate and the synthesis of thymidylate from deoxyuridylate. 1-Deoxy- D-xylulose 5-phosphate reductoisomerase (PDB ID: 3WQR) catalyzes an essential step in the non-mevalonate pathway of isoprenoid biosynthesis [65]. NADH dehy- drogenase (PDB ID: 5JWC) is part of the mitochondrial electron transport chain, and it catalyzes the transfer of electrons from NADH to ubiquinone [66]. Hexose trans- porter 1 (PDB ID: 6M2L) facilitates the transport of glu- cose across the plasma membrane [67].

Since the antiplasmodial flavonoid quercetin was found to be present in *D. Sissoo*, which also happens to be traditionally used as a herbal remedy for the treatment of malaria, we used the network pharmacology tech- nique to understand the molecular mechanism of action of quercetin against malaria. In addition, this will help us to have some understanding of how *D. Sissoo* was able to alleviate malaria. The network pharmacol- ogy technique has several applications in the field of drug repurposing, identification of gene targets, and identifi- cation of the molecular mechanism of action [68, 69]. From a total of 27 common targets between quercetin and malaria, the ranking algorithm 'degree' has identified 10 hub genes (Fig. 11). Hub genes are highly connected genes that play an important role in the maintenance of biological networks [70]. For the protein–protein interac- tion network analysis, we used 'degree' which counts the number of edges (direct connections) a node (gene) has.

The GO enrichment analysis of the hub genes revealed the most significant BP (inflammatory response), CC (extracellular space), and MF (cytokine activity) (Fig. 12). BP refers to the contribution of the genes toward a bio- logical activity, CC provides the cellular location where the gene is active, and MF indicates the molecular activ- ity of the gene [71]. Pathway enrichment analysis revealed that the hub genes were significantly overrepresented in malaria followed by other diseases (Fig. 13). Furthermore,

Journal of Molecular Science
Volume 35 Issue 4, Year of Publication 2025, Page 1678-1698
DoI-10.004687/1000-9035.2025.219

Reactome analysis revealed that IL-4 and IL-13 signaling, IL-10 signaling, signaling by interleukins, and cytokine signaling in the immune system were significantly more prominent (Fig. 13). IL-4 is a cytokine that facilitates the differentiation of T cells into Th2 cells and stimulates B cells to produce immunoglobulin E [72]. IL-10 inhibits the production of pro-inflammatory cytokines such as IL-1, IL-6, IL-12, and TNF-α [73]. IL-13 functions simi- larly to IL-4 and plays a role in tissue repair [72]. The GO enrichment analysis (Fig. 12) and pathway enrichment analysis (Fig. 13) showed positive correlations. The genes that could be potentially affected by quercetin in the malaria pathway are highlighted in pink color (Fig. 14). Although our findings are limited at the *in silico* level, the network pharmacology studies provided promis- ing results with strong indications for quercetin against malaria.

CONCLUSIONS:

The pharmacognostic parameters of the bark of *D. Sissoo* have been reported for the first time in this study. These parameters, including the FT-IR fingerprint and the HPTLC fingerprint, can be used as a referen- tial herbal monograph to aid in identification, maintain purity, detect adulteration, and control the quality of crude drugs and their extracts. The presence of quercetin in the 80% MeOH bark extract of *D. Sissoo* has been reported for the first time through a validated HPTLC densitometric method. The developed HPTLC method can be used as a standardization technique for the crude drugs obtained from the bark of *D. Sissoo*. The QSAR-based IC_{50} prediction and other previous studies confirmed that quercetin exhibits antiplasmodial activ- ity against *P. falciparum*. With a new style of approach for protein retrieval, we were able to target *P. falciparum* proteins that are highly expressed during the trophozoite and schizont stages. Molecular docking studies revealed that quercetin could inhibit *P. falciparum* by binding to several proteins that are crucial for the maintenance of the normal metabolic process. Through network pharma- cology, we found that quercetin could potentially allevi- ate malaria by regulating the pro-inflammatory response through the action of IL-4, IL-10, and IL-13, and by trig- gering the immune system. The results obtained from the network pharmacology study support the use of *D. Sissoo* as a traditional herbal remedy against malaria.

Abbreviations:

FT-IR Fourier transform infrared
HPTLC High-performance thin-layerchromatography
WHO World Health Organization
GGACP Guidelines on good agricultural and collection practices
TS Transverse section
UV Ultraviolet
ICH International Conference on Harmonization
QSAR Quantitative structure–activity relationship
2D 2-Dimensional
TDR Tropical disease research
PDB Protein data bank
DSV Discovery Studio Visualizer
CCIs Co-crystal inhibitors
GO Gene ontology
BP Biological process
MF Molecular functions
CC Cellular compartments
Rf Retention factor
IC50 Half-maximal inhibitory concentration
RMSD Root-mean-squared deviation

ACKNOWLEDGEMENTS:

Dr. Pradip Ghogare is thankful SMBT College of Pharmacy Dhamangaon Tal.Igatpuri Dist. Nashik (M.S.) India for providing necessary facility to complete research work.

AUTHOR CONTRIBUTIONS:

PBG, SVL, BDT prepared the study design. PBG carried out the Pharmacognostical works. PBG and SVL carried out the HPTLC studies. VSB and NAN carried out *in vitro* antimalarial screening. SVL carried out multi-target molecular docking studies. PBG and NAN carried out the network pharmacology studies. SVL supervised PBG for the preparation of the images and drafting of the manuscript.

FUNDING:

Not applicable.

DECLARATIONS:

Ethics approval and consent to participate:

Not applicable.

Consent for publication:

Not applicable.

Competing interests:

The authors declare no competing interests.

Statement on studies involving plants:

The WHO guidelines for good agricultural and collection practices were followed. The plant parts were taxonomically authenticated Botanist

Author details:

[1]Department of Pharmacognosy, SMBT College of Pharmacy, Dhamangaon, Tal. Igatpuri Dist. Nashik. (M.S.)

References:

1. Rizwan S, Hanley T, Boyd B et.al crystalline systems of phytantriol and glyceryl monooleate containing a hydrophilic protein: characterisation, swelling and release kinetics. J Pharm Sci 2009; 98: 4191-204.
2. Lakhey, P.; Pathak, J.; Adhikari, B. (2020). "Dalbergia sissoo".

IUCN Red List of Threatened Species 19 November 2021
3. Lalramnghinglova H (2016) Documentation of Medicinal Plants based on Traditional Practices in the Indo- Burma Hotspots Region of Mizoram, North East India. Emer Life Sci Res 2:10–45
4. Khiangte Z (2017) Documentation of plants used in traditional medicines and practices in Mizoram. Available via Digital Repository, Mizoram University. https://mzuir.inflibnet.ac.in/handle/123456789/329?mode= full. Accessed 25 Sept 2020.
5. Kshetrimayum B (2017) Medicinal Plants and Its Therapeutic Uses. OMICS International, India
6. Pongamornkul W, Muangyen N, Phookaphin B, Panyadee P, Inta A (2020) Ethnomedicinal Knowledge of Pwo People in Northern Thailand. https:// doi.org/10.21203/rs.3.rs-21537/v1 (preprint)
7. Dangar DK, Patel NJ (2020) Pharmacognostic studies on Neuracanthus sphaerostachyus Dalz. (Acanthaceae) leaves. J Ayurveda Integr Med 11:529–533
8. Kabra A, Sharma R, Singla S, Kabra R, Baghel US (2019) Pharmacognos- tic characterization of Myrica esculenta leaves. J Ayurveda Integr Med 10:18–24
9. Megawati E, Bangun H, Putra I, Rusda M, Syahrizal D, Jusuf NK, Eyanoer PC, Lubis RR, Amin MM (2023) Phytochemical Analysis by FTIR of Zanth- oxylum Acanthopodium, DC Fruit Ethanol Extract, N-hexan, Ethyl Acetate and Water Fraction. Med Arch 77:183
10. Pareek SS, Vijayvargia P, Jha SK, Khandelwal D, Vijayvergia R (2023) HPTLC based quantification of β-sitosterol from the leaves of Nyctanthes arbor- tristis and in-silico prediction of potential drug targeted towards cancer therapy. J Biomol Struct Dyn. https://doi.org/10.1080/07391102.2023. 2275171
11. Agatonovic-Kustrin S, Gegechkori V, Petrovich DS, Ilinichna KT, Morton DW (2021) HPTLC and FTIR Fingerprinting of Olive Leaves Extracts and ATR-FTIR Characterisation of Major Flavonoids and Polyphenolics. Mol- ecules 26:6892
12. Zothantluanga J, Aswin SK, Rudrapal M, Chetia D (2021) Antimalarial Fla- vonoid-Glycoside from Acacia pennata with Inhibitory Potential Against PfDHFR-TS: An In-silico Study. Biointerface Res Appl Chem 12:4871–4887
13. World Health Organization (2024) World Malaria Report 2023. https:// www.who.int/teams/global-malaria-programme/reports/world-malaria- report 2023. Accessed 5 July 2024.
14. Adebayo AH, Ishola TA, Yakubu OF (2021) Acute toxicity and antima- larial studies of extract of Allophylus spicatus in animals. Toxicol Res 37:345–354
15. Sarma M, Abdalla M, Zothantluanga JH, Abdullah Thagfan F, Umar AK, Chetia D, Almanaa TN, Al-Shouli ST (2023) Multi-target molecular
16. dynamic simulations reveal glutathione-S-transferase as the most favora- ble drug target of knipholone in Plasmodium falciparum. J Biomol Struct Dyn 41:12808–12824
17. Pathak K, Pathak MP, Saikia R, Gogoi U, Sahariah JJ, Zothantluanga JH, Samanta A, Das A (2022) Cancer Chemotherapy via Natural Bioactive Compounds. Curr Drug Discov Technol 19:e310322202888
18. Appiah-Opong R, Agyemang K, Dotse E, Atchoglo P, Owusu KB-A, Aning A, Sakyiamah M, Adegle R, Ayertey F, Appiah AA, Nyarko AK (2022) Anti- plasmodial, Cytotoxic and Antioxidant Activities of Selected Ghanaian Medicinal Plants. J Evidence-Based Integr Med 27:2515690X2110737.
19. Ferreira LT, Borba JVB, Moreira-Filho JT, Rimoldi A, Andrade CH, Costa FTM (2021) QSAR-Based Virtual Screening of Natural Products Database for Identification of Potent Antimalarial Hits. Biomolecules 11:459
20. Umar AK, Roy D, Abdalla M, Modafer Y, Al-Hoshani N, Yu H, Zothantluanga JH (2023) In-silico screening of Acacia pennata and Bridelia retusa reveals pinocembrin-7-O-β-D-glucopyranoside as a promising β-lactamase inhibitor to combat antibiotic resistance. J Biomol Struct Dyn. https://doi.org/10.1080/07391102.2023.2248272
21. Dai H, Shan Y, Yu M, Wang F, Zhou Z, Sun J, Sheng L, Huang L, Sheng M (2024) Network pharmacology, molecular docking and experimental verification of the mechanism of huangqi-jixuecao herb pair in treatment of peritoneal fibrosis. J Ethnopharmacol 318:116874
22. Zothantluanga JH, Sailo N, Paul A, Shakya A (2020) Pharmacognostical characterization and in vitro antioxidant activity of Acacia pennata (L.) Willd. leaves: A Southeast Asian medicinal plant. Sci Vis 20:16–28
23. Kokate C, Purohit A, Gokhale S (2018) Pharmacognosy. Pune, India
24. Indian Pharmacopoeial Commision (2018) Tests on herbal products. Indian Pharmacopoeia, India
25. Vk K, Lalitha K (2017) Pharmacognostical and phytochemical studies of Helleborus niger L root. Anc Sci Life 36:151
26. Khandelwal KR (2008) Practical pharmacognosy: techniques and experi- ments. Nirali Prakashan, India
27. Wongsa P, Phatikulrungsun P, Prathumthong S (2022) FT-IR characteristics, phenolic profiles and inhibitory potential against digestive enzymes of 25 herbal infusions. Sci Rep 12:6631
28. Srinivas A, Nehra S (2024) Development of HPTLC method for simultane- ous determination of quercetin and kaempferol in leaf extract of Hibiscus mutabilis. J Chromatogr B 1246:124277
29. Gogoi N, Gogoi B, Chetia D (2021) In vitro antimalarial activity evaluation of two ethnomedicinal plants against chloroquine sensitive and resistant strains of Plasmodium falciparum. Clin Phytoscience 7:42
30. Pandey AK, Sharma S, Pandey M, Alam MM, Shaquiquzzaman M, Akhter M (2016) 4, 5-Dihydrooxazole-pyrazoline hybrids: Synthesis and their evaluation as potential antimalarial agents. Eur J Med Chem 123:476–486
31. Zothantluanga JH, Chetia D, Rajkhowa S, Umar AK (2023) Unsupervised machine learning, QSAR modelling and web tool development for streamlining the lead identification process of antimalarial flavonoids. SAR QSAR Environ Res 34:117–146
32. Babai R, Izrael R, Vértessy BG (2022) Characterization of the dynamics of Plasmodium falciparum deoxynucleotide-triphosphate pool in a stage- specific manner. Sci Rep 12:19926
33. Urán Landaburu L, Berenstein AJ, Videla S, Maru P, Shanmugam D, Cher- nomoretz A, Aguero F (2019) TDR Targets 6: driving drug discovery for human pathogens through intensive chemogenomic data integration. Nucleic Acids Res 48:992–1005
34. Zothantluanga JH, Aswin SK, Rudrapal M, Cheita D (2022) Antimalarial flavonoid-glycoside from acacia pennata with inhibitory potential against PfDHFR-TS: An in-silico study. Biointerface Res Appl Chem 12:4871–4887
35. Arefin A, Ismail Ema T, Islam T, Saddam Hossen M, Islam T, Al Azad S, Uddin Badal N, Islam A, Biswas P, Alam NU, Islam E, Anjum M, Masud A, Kamran S, Rahman A, Kumar Paul P (2021) Target specificity of selective bioactive compounds in blocking α-dystroglycan receptor to suppress Lassa virus infection: an in silico approach. J Biomed Res 35:459
36. Nipun T, Ema T, Mia M, Hossen M, Arshe F, Ahmed SZ, Masud A, Taheya FF, Khan AA, Haque F, Azad SA, Al Hasibuzzaman M, Tanbir M, Anis S, Akter
37. S, Mily SJ, Dey D (2021) Active site-specific quantum tunneling of hACE2 receptor to assess its complexing poses with selective bioactive com- pounds in co-suppressing SARS-CoV-2 influx and subsequent cardiac injury. J Adv Vet Anim Res 8(4):540–556
38. Zothantluanga JH, Umar AK, Aswin K, Rajkhowa S, Chetia D (2023) Revelation of potential drug targets of luteolin in Plasmodium falciparum through multi-target molecular dynamics simulation studies. J Biomol Struct Dyn. https://doi.org/10.1080/07391102.2023.2263875
39. Dallakyan S, Olson AJ (2015) Small-Molecule Library Screening by Dock- ing with PyRx. Methods Mol Biol 1263:243–250
40. Paul P, Azad S, Rahman M, Farjana M, Uddin M, Dey D,

Journal of Molecular Science
Volume 35 Issue 4, Year of Publication 2025, Page 1678-1698
DoI-10.004687/1000-9035.2025.219

Mahmud S, Ema TI, Biswas P, Anjum M, Akhi OJ, Ahmed SZ (2022) Catabolic profiling of selective enzymes in the saccharification of non-food lignocellulose parts of biomass into functional edible sugars and bioenergy: An in silico bioprospecting. J Adv Vet Anim Res 9:19–32

41. Ferdausi N, Islam S, Rimti F, Quayum S, Arshad E, Ibnat A, Islam T, Arefin A, Ema TI, Biswas P, Dey D, Azad SA (2022) Point-specific interactions of
42. isovitexin with the neighboring amino acid residues of the hACE2 recep- tor as a targeted therapeutic agent in suppressing the SARS-CoV-2 influx mechanism. J Adv Vet Anim Res 9:230–240
43. Dey D, Paul P, Azad S, Mazid M, Khan A, Sharif M, Rahman MH (2021) Molecular optimization, docking, and dynamic simulation profiling of selective aromatic phytochemical ligands in blocking the SARS-CoV-2 S protein attachment to ACE2 receptor: an in silico approach of targeted drug designing. J Adv Vet Anim Res 8:24–35
44. Jabin A, Uddin MF, et.al (2023) Target-specificity of different amyrin subunits in impeding HCV influx mechanism inside
45. the human cells considering the quantum tunnel profiles and molecular strings of the CD81 receptor: a combined in silico and in vivo study. In- Silico Pharmacol 11:8
46. Bell EW, Zhang Y (2019) DockRMSD: an open-source tool for atom mapping and RMSD calculation of symmetric molecules through graph isomorphism. J Cheminform 11:40
47. Morshed AKMH, Al Azad S, Mia MAR, Uddin MF, Ema TI, Yeasin RB, Srishti SA, Sarker P, Aurthi RY, Jamil F, Samia NSN, Biswas P, Sharmeen IA, Ahmed R, Siddiquy M, Nurunnahar, (2023) Oncoinformatic screening of the genclusters involved in the HER2-positive breast cancer formation along with the in silico pharmacodynamic profiling of selective long-chain omega-3 fatty acids as the metastatic antagonists. Mol Divers 27:2651–2672
48. Rahman MH, Al Azad S, Uddin MF, Farzana M, Sharmeen IA, Kabbo KS, Jabin A, Rahman A, Jamil F, Srishti SA, Riya FH, Khan T, Ahmed R, Nurun- nahar RS, Khan MFR, Rahman MB (2023) WGS-based screening of the co-chaperone protein DjlA-induced curved DNA binding protein A (CbpA) from a new multidrug-resistant zoonotic mastitis-causing Klebsiella pneumoniae strain: a novel molecular target of selective flavonoids. Mol Divers. https://doi.org/10.1007/s11030-023-10731-6
49. Parzhanova A, Yanakieva V, Vasileva I, Momchilova M, Dimitrov D, Ivanova P, Tumbarski Y (2023) Physicochemical, Antioxidant, and Antimicrobial Properties of Three Medicinal Plants from the Western Part of the Rho- dope Mountains. Bulgaria Life 13:2237
50. Kamboj A, Saluja AK (2017) Development of validated HPTLC method for quantification of stigmasterol from leaf and stem of Bryophyllum pin- natum. Arab J Chem 10:2644–2650
51. Cornara L, Smeriglio A, Frigerio J, Labra M, Di Gristina E, Denaro M, Mora E, Trombetta D (2018) The problem of misidentification between edible and poisonous wild plants: Reports from the Mediterranean area. Food Chem Toxicol 119:112–121
52. Fitzgerald M, Heinrich M, Booker A (2020) Medicinal Plant Analysis: A Historical and Regional Discussion of Emergent Complex Techniques. Front Pharmacol 10:1480
53. de Medeiros PM, Santos Pinto BL, do Nascimento VT, (2015) Can organoleptic properties explain the differential use of medicinal plants? Evidence from Northeastern Brazil. J Ethnopharmacol 159:43–48
54. Woolfson KN, Esfandiari M, Bernards MA (2022) Suberin Biosynthesis, Assembly, and Regulation. Plants 11:555
55. Mukhi S, Bose A, Panda P, Rao MM (2016) Pharmacognostic, physico- chemical and chromatographic characterization of Samasharkara Churna. J Ayurveda Integr Med 7:88–99
56. Gempo N, Yeshi K, Jamtsho T, Jamtsho L, Samten, Wangchuk P (2024) Development of quality control parameters for two Bhutanese medicinal plants (Aster flaccidus Bunge and Aster diplostephioides (DC.) Benth. ex C.B.Clarke) using traditional and modern pharmacognostical platforms. Heliyon 10:e24969.
57. Liu K (2022) New and improved methods for measuring acid insoluble ash. Anim Feed Sci Technol 288:115282
58. Prakash A, Janmeda P, Pathak P, Bhatt S, Sharma V (2019) Development and standardization of quality control parameters of different parts of Trianthema portulacastrum L. SN Appl Sci 1:1108
59. Hameed A, Ghani N, Mughal TA, Abbas M, Abrar A, Javed H (2023) Phar- macognostical evaluation and physiochemical analysis of Salsola Kali as medicinal plant. Microsc Res Tech 86:1322–1332
60. Alam F, Us Saqib Q (2015) Pharmacognostic study and development of quality control parameters for fruit, bark and leaf of Zanthoxylum arma- tum (Rutaceae). Anc Sci Life 34:147
61. Singh PK, Singh J, Medhi T, Kumar A (2022) Phytochemical Screening, Quantification, FT-IR Analysis, and In Silico Characterization of Potential Bio-active Compounds Identified in HR-LC/MS Analysis of the Polyherbal Formulation from Northeast India. ACS Omega 7:33067–33078
62. Karthika K, Paulsamy S (2015) TLC and HPTLC fingerprints of various secondary metabolites in the stem of the traditional medicinal climber, solena amplexicaulis. Indian J Pharm Sci 77:111
63. Itankar P, Sawant D, Tauqeer M, Charde S (2015) High performance thin layer chromatography fingerprinting, phytochemical and physico-chem- ical studies of anti-diabetic herbal extracts. AYU (An Int Q J Res Ayurveda) 36:188
64. Chaniad P, Mungthin M, Payaka A, Viriyavejakul P, Punsawad C (2021) Antimalarial properties and molecular docking analysis of compounds from Dioscorea bulbifera L. as new antimalarial agent candidates. BMC Complement Med Ther 21:144.
65. Adeoye AO, Olanlokun JO, Tijani H, Lawal SO, Babarinde CO, Akinwole MT, Bewaji CO (2019) Molecular docking analysis of apigenin and quercetin from ethylacetate fraction of Adansonia digitata with malaria-associated calcium transport protein: An in silico approach. Heliyon 5:e02248
66. Hasan MM, Khan Z, Chowdhury MS, Khan MA, Moni MA, Rahman MH (2022) In silico molecular docking and ADME/T analysis of Quercetin compound with its evaluation of broad-spectrum therapeutic potential against particular diseases. Informatics Med Unlocked 29:100894
67. Zothantluanga JH, Chetia D (2022) A beginner's guide to molecular dock- ing. Sci Phytochem 1:37–40
68. Umar AK, Zothantluanga JH, Aswin K, Maulana S, Sulaiman Zubair M, Lalhlenmawia H, Rudrapal M, Chetia D (2022) Antiviral phytocompounds "ellagic acid" and "(+)-sesamin" of Bridelia retusa identified as potential inhibitors of SARS-CoV-2 3CL pro using extensive molecular docking, molecular dynamics simulation studies, binding free energy calculations, and bioactivity prediction. Struct Chem 33(5):1445–1465
69. Rasina D, Otikovs M, Leitans J, Recacha R, Borysov OV, Kanepe-Lapsa I, Domraceva I, Pantelejevs T, Tars K, Blackman MJ, Jaudzems K, Jirgensons A (2016) Fragment-Based Discovery of 2-Aminoquinazolin-4(3 H)-ones As Novel Class Nonpeptidomimetic Inhibitors of the Plasmepsins I, II, and IV. J Med Chem 59:374–387
70. Konzuch S, Umeda T, Held J, Hähn S, Brücher K, Lienau C, Behrendt CT, Gräwert T, Bacher A, Illarionov B, Fischer M, Mordmüller B, Tanaka N, Kurz T (2014) Binding Modes of Reverse Fosmidomycin Analogs toward the Antimalarial Target IspC. J Med Chem 57:8827–8838
71. Yang Y, Yu Y, Li X, Li J, Wu Y, Yu J, Ge J, Huang Z, Jiang L, Rao Y, Yang M (2017) Target Elucidation by Cocrystal Structures of NADH-Ubiquinone Oxidoreductase of Plasmodium falciparum (Pf NDH2) with Small Mol- ecule To Eliminate Drug-Resistant Malaria. J Med Chem 60:1994–2005
72. Jiang X, Yuan Y, Huang J, Zhang S, Luo S, Wang N, Pu D, Zhao N, Tang Q, Hirata K, Yang X, Jiao Y, Sakata-Kato T, Wu JW, Yan C, Kato N, Yin H, Yan N (2020) Structural Basis for Blocking Sugar Uptake into the Malaria Parasite Plasmodium

Journal of Molecular Science
Volume 35 Issue 4, Year of Publication 2025, Page 1678-1698
DoI-10.004687/1000-9035.2025.219

falciparum. Cell 183:258–268
73. An W, Huang Y, Chen S, Teng T, Shi Y, Sun Z, Xu Y (2021) Mechanisms of Rhizoma Coptidis against type 2 diabetes mellitus explored by network pharmacology combined with molecular docking and experimental validation. Sci Rep 11:20849
74. Obaidullah AJ, Alanazi MM, Alsaif NA, Alanazi AS, Albassam H, Az A, Alwassil OI, Alqahtani AM, Tareq AM (2022) Network Pharmacology- and Molecular Docking-Based Identification of Potential Phytocompounds from Argyreia capitiformis in the Treatment of Inflammation. Garg R, edi- tor. Evidence-Based Complement Altern Med 2022:8037488.
75. Das S, Meher PK, Rai A, Bhar LM, Mandal BN (2017) Statistical Approaches for Gene Selection, Hub Gene Identification and Module Interaction
76. in Gene Co-Expression Network Analysis: An Application to Aluminum Stress in Soybean (Glycine max L.). Tian Z, editor. PLoS One 12:e0169605.
77. Kim TH, Yu GR, Kim H, Kim JE, Lim DW, Park WH (2023) Network Pharma- cological Analysis of a New Herbal Combination Targeting Hyperlipi- demia and Efficacy Validation In Vitro. Curr Issues Mol Biol 45:1314–1332
78. Junttila IS (2018) Tuning the Cytokine Responses: An Update on Interleu- kin (IL)-4 and IL-13 Receptor Complexes. Front Immunol. https://doi.org/ 10.3389/fimmu.2018.00888
79. Kessler B, Rinchai D, Kewcharoenwong C, Nithichanon A, Biggart R, Haw- rylowicz CM, Bancroft GJ, Lertmemongkolchai G (2017) Interleukin 10 inhibits pro-inflammatory cytokine responses and killing of Burkholderia pseudomallei. Sci Rep 7:42791